Antragstyp	Schwerpunktprogramm - Einzelantrag - Neuantrag
Type of Proposal	Priority Programme - Individual Proposal - New Proposal
Antragsdauer / Requested Duration	36 Monate / 36 months
Fach	Strömungsmechanik
Subject Area	Fluid Mechanics
Rahmenprojekt / Framework Project	SPP 2171
Titel	**Direkte numerische Simulation von aufprallenden Tropfen auf elastischen Grenzflächen**
Title	**Direct numerical simulation of droplet impacts with an elastic fluidic interface**
Geschäftszeichen / Reference No.	**LE 3303/4-1**
Antragsteller / Applicant	**Dr. Gregory Lecrivain, Ph.D.** Helmholtz-Zentrum Dresden-Rossendorf (HZDR) Institut für Fluiddynamik Dresden

Beantragte Mittel / Budget Request:

	Beantragt / Requested		
Dauer [Monate] / Duration [Months]			**36**
LE 3303/4-1			
Summe / Total [Euro]			**158.043**
Dr. Gregory Lecrivain, Ph.D.			
	Anz. / No.	**Dauer / Duration**	**Euro**
Personalmittel / Funding for Staff			**149.793**
Doktorandin/Doktorand und Vergleichbare 75 % / Doctoral Researcher or Comparable 75 %	1	36	145.100
Hilfskräfte / Support Staff			4.693
Sachmittel / Direct Project Costs			**8.250**
Geräte bis 10.000 Euro, Software und Verbrauchsmaterial / Equipment up to EUR 10,000, Software and Consumables			1.000
Publikationen / Publications			2.250

Reisen / Travel			5.000

Zusammenfassung

Das Aufprallen eines Tropfens mit niedriger kinetischer Energie auf ein elastisches Substrat tritt in vielen industriellen Anwendungen, wie beispielsweise beim Tintenstrahldruckverfahren und bei der Geweberekonstruktion durch „Tissue Engineering“, auf. Die Dynamik von aufprallenden Tropfen auf einem harten Substrat ist inzwischen gut verstanden und wurde mithilfe von direkten numerischen Simulationen berechnet. Der Tropfenaufprall auf ein elastisches Substrat ist dagegen bis heute kaum untersucht worden. Ziel des Vorhabens ist es, die dynamische Wechselwirkung zwischen aufprallenden Tropfen und einem fluidischen, elastischen Substrat zu modellieren und zu simulieren. Der Tropfenaufprall auf Oberflächen, die mit einem dünnen Flüssigkeitsfilm bedeckt sind, wie z.B. mit Öl versetzte texturierte Materialoberflächen (eng. lubricant-infused surfaces), sowie auf freistehenden smektischen Filmen, werden im Rahmen dieses Schwerpunktprogramms von Partnern experimentell untersucht. Dabei sorgt das flüssige Substrat für eine elastisch rückwirkende Kraft und die Viskosität des umgebenden Fluids für eine dämpfende Kraft. Ein Dreiphasenmodell, basierend auf der Phasenfeldtheorie, wird weiterentwickelt und soll für die Simulation von einzelnen und mehreren oszillierenden Tropfen angewendet werden. Mithilfe von direkten numerischen Simulationen wird ein substantieller Beitrag zum besseren Verständnis der Dynamik von aufprallenden Tropfenensembles auf einem elastischen Substrat geleistet.

Summary

The low-energy impact of a liquid droplet with an elastic substrate is a ubiquitous phenomenon occurring in various industrial applications. Notable examples include ink-jet printing and tissue engineering. The droplet impact with a hard substrate is now well understood and has been studied for over a century. Various direct numerical simulations have also been performed. The numerical investigation of a droplet impacting with an elastic substrate has, however, received much less attention. This project aims at simulating the complex interaction between impacting droplets and an elastic fluidic substrate. Hard surfaces covered by a thin liquid film, such as oil-infused surfaces, and freestanding smectic films, will be considered. The droplet impact with such substrates will also be investigated experimentally by partners involved in this priority programme. In such experiments, the fluidic substrate acts as restoring force, while the viscosity of the ambient fluid acts as a damping force. The further development of a ternary fluid model, based on the phase field theory, will allow the direct numerical simulation of single and multiple oscillating droplets. Results of this study will contribute to a better understanding of the dynamics of droplet ensembles impacting with an elastic substrate.

Project Description – Project Proposals

Applicant: Dr. Grégory Lecrivain, Helmholtz-Zentrum Dresden-Rossendorf, Institute for Fluid Dynamics, Bautzner Landstraße 400, 01328 Dresden, Germany

Title: Direct numerical simulation of droplet impacts with an elastic fluidic interface

1 State of the art and preliminary work

The wetting and the dewetting properties of a substrate are of upmost important to many natural and technological applications. The substrates considered in this priority programme can either be ***flexible, adaptive, or switchable***. A flexible substrate, such as a lubricant-infused surface, will deform because of the traction exerted by a liquid droplet in contact with the thin liquid film. The droplet in-turn experiences an altered geometry. An adaptive substrate will change its physico-chemical properties due to the presence of a liquid. A switchable substrate, such as a photoswitchable surface, will alter its surface properties upon exposure to an external influence. The present research proposal falls under the category of deformable substrates. The combined interaction between an impacting fluid droplet and a liquid film, acting as flexible substrate, is here of particular interest. Figure 1 shows how the candidate's work is embedded into this priority programme. The collaborative three work packages (WP) and the interaction with other members are also shown.

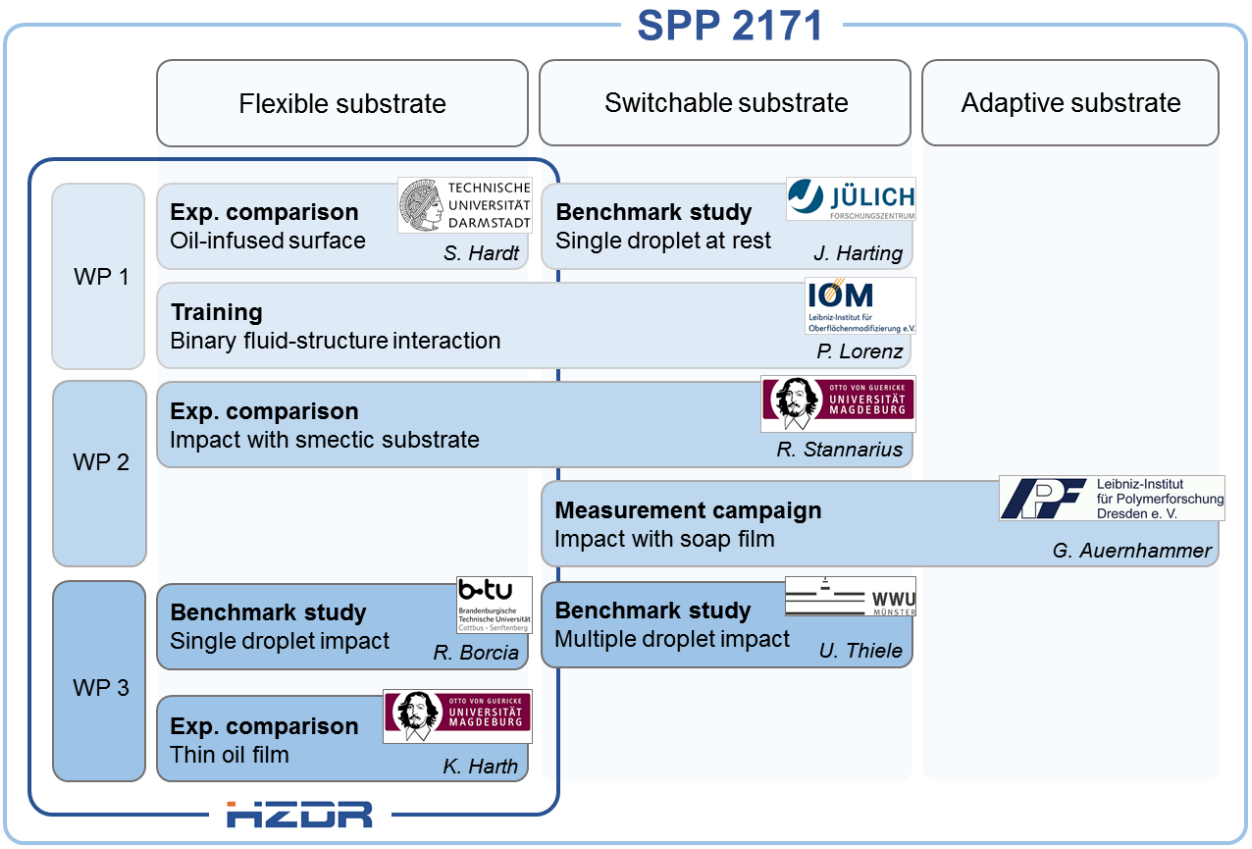

***Fig. 1**: Collaborative work between HZDR and the partner institutions involved in the priority programme. The cooperations include three comparisons to experimental data, three numerical benchmarks, one measurement campaign and one advanced training organised by the principal investigator.*

1.1 State of the art

A fluidic substrate (or fluidic interface) indicates here an interfacial surface separating two fluids. Examples of natural and industrial fluidic substrates include a hard substrate covered with a thin liquid film [A1, A2], soap surfactant films [A3, A4], smectic films [A5], oil-water interfaces [A6], and vibrating air-oil interfaces [A7]. Two prominent examples relevant to this priority programme are presented below to illustrate the striking resemblance between the dynamics of a fluidic interface and those of a solid (visco)elastic substrate.

1.1.1 Droplet sliding down a fluidic substrate

The first example consists of a liquid droplet sliding down an incline. On a solid substrate, the droplet is normally subject to large friction forces. To enhance the droplet mobility, a thin lubrication layer of fluid may be applied onto the solid substrate [A8]. This particular type of fluidic substrates, known as ***lubricant-infused surfaces*** [A9, A10], involves a hydrophobic micro-texturing of the solid, onto which a thin layer of lubricant, such as oil, is entrapped. A sketch is illustrated in Figure 2. A water droplet slides down the lubricant-infused surface with a much lower resistance. Owing to its lowered wall friction, this type of substrate finds application in microfluidic systems, where energy consumption can be significantly reduced [A11, A12]. As seen in the two subfigures on the right, the local deformation of the fluidic substrate at the three-phase contact line is reminiscent to that of a solid viscoelastic substrate [A13]. Experimental evidence showed that, when a solid substrate is sufficiently soft to be deformed by the capillary action, its initially flat surface locally deforms into a sharp ridge near the three-phase contact line [A14]. The liquid drop is said to “surf” the ridge [A15].

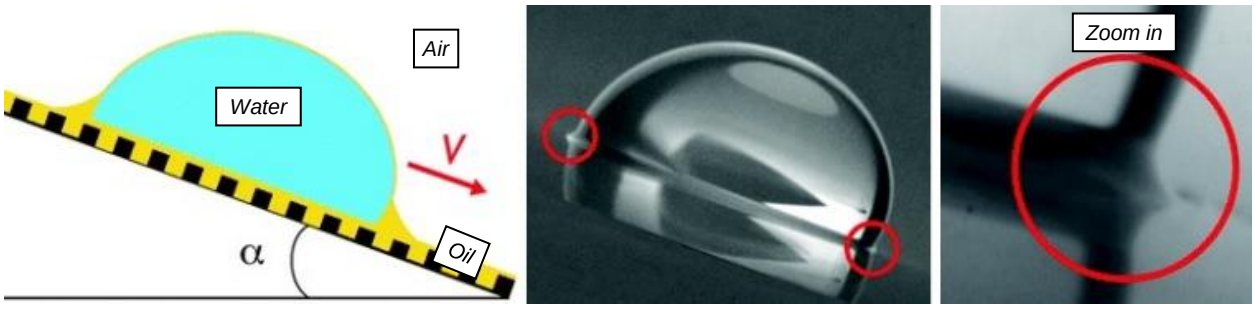

Fig. 2*: The left subfigure shows a schematic of a lubricant-infused surface onto which a liquid droplet slides down [A11]. In the right subfigures [A10], the local deformation of the oil-air fluidic interface at the three-phase contact line is identical to that observed for a “solid” substrate made of a soft gel-like material.*

1.1.2 Droplet bouncing on a fluidic substrate

The second example is concerned with the low-energy impact of a droplet with an elastic substrate [A16]. Droplet impact is a ubiquitous phenomenon occurring in various natural and industrial applications. Notable industrial examples include ink-jet printing and tissue engineering [A16-19]. Figure 3 shows the successive impacts of an oscillating droplet with various fluidic substrates, a mechanism known as the trampoline effect [A3, A4, A20]. In the presented three cases, the fluidic substrate behaves just like a spring. ***The surface tension of the fluidic substrate acts as restoring force while the viscosity of the ambient fluid acts as a damping force***. The vertical position $y(t)$ of the droplet oscillating on a fluidic substrate can be accurately modelled by solving a one-dimensional spring-equation of the type

$$m\frac{\mathrm{d}^2y}{\mathrm{d}t^2} + k\frac{\mathrm{d}y}{\mathrm{d}t} = -mg + F_{\mathrm{fl}\to\mathrm{d}}, \tag{1}$$

where m is the mass of the droplet, k a drag force coefficient, g the gravity, and $F_{\mathrm{fl}\to\mathrm{d}}$ the elastic force exerted by the fluidic interface onto the droplet [A21]. The dynamics of a single droplet bouncing off a fluidic substrate are identical to those already reported for a “solid” elastic substrate coated with a super-hydrophobic layer [A22, A23]. In both cases, a portion of the total energy is

turned into an elastic contribution associated with the substrate deformation, from which a restitution coefficient can be derived.

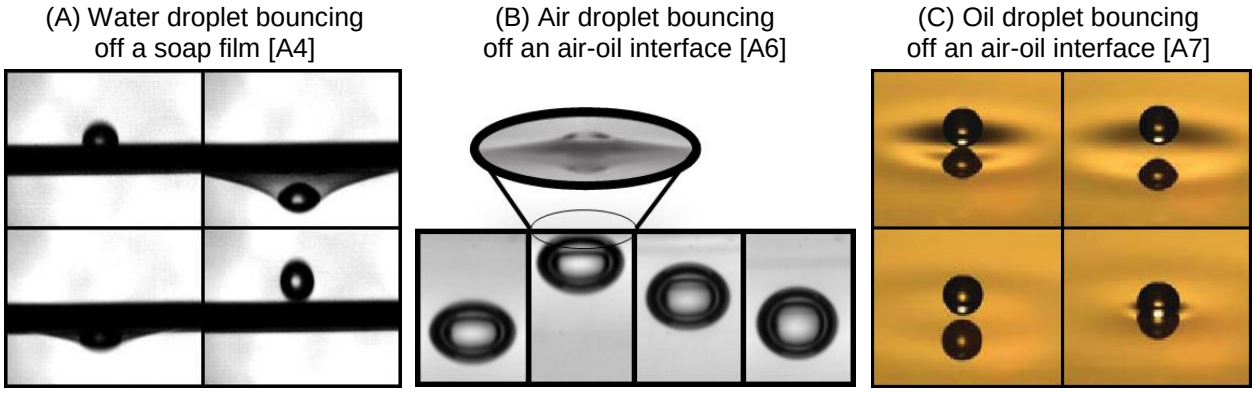

Fig. 3*: Exemples showcasing the successive impacts of an oscillating droplet with a fluidic substrate. In (A), the water droplet impacts and then bounces off a freestanding soap film. In (B), an air bubble rises, impacts, and then bounces off a oil-air interface. In (C), an oil droplet keeps impacting with the oil-air interface of a vibrating bath.*

1.1.3 Direct numerical simulation of a liquid droplet interacting with a hard substrate

Despite its rich and remarkable dynamics, literature data on the direct numerical simulation of a droplet interacting with a fluidic substrate is relatively scarce. This is probably attributed to the complexity of the model development, in which substrate deformation, capillary effects, and multiphase flow hydrodynamics are intertwined. Consequently, a selection of recent numerical advancements, which treats the dynamics of a droplet impinging on a hard substrate, is presented. This brief review on the current state of the art will inspire the numerical activities suggested in the research plan. The numerical investigation of the droplet impact with a hard solid substrate, be it a horizontal or an inclined surface, is now fairly well documented [A24-26]. Yet, it continues to be an active research field. Recent works include the direct numerical simulation of droplet splashing [A27] and droplet bouncing off a textured super-hydrophobic substrate [A28]. Snapshots of the three-dimensional simulations are shown in Figure 4 for low and high Weber numbers. The Weber number, defined as the ratio of the kinetic energy upon impact to the surface energy, is defined as $\mathrm{We} = \rho_\mathrm{A} U_b d_b / \gamma$, where ρ_A is the density of the ambient fluid, U_b the impact droplet velocity, d_b the droplet diameter, and γ the surface tension.

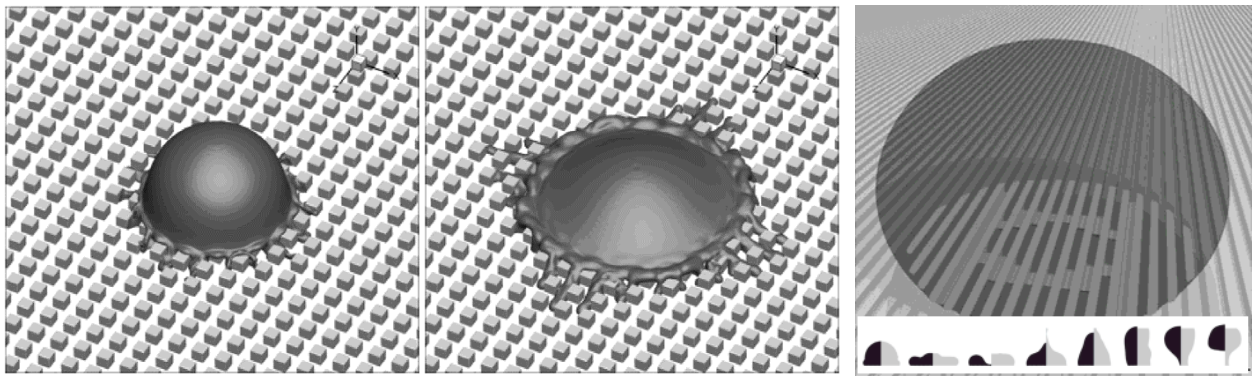

Fig. 4*: Left: splashing of a droplet on a textured surface at high Weber number [A27]. Right: at low Weber number, the droplet rebound occurs [A28]. A time sequence (bottom right) compares the simulated contour of the rebounding droplet (black) with the experimental data (grey).*

Further direct numerical simulations on single droplets impacting with a textured substrate can be found in Reference [A29]. Direct numerical simulations of a droplet bouncing off a flat surface with

varying wettability were also recently reported by Raman et al. [A30]. The spatial inhomogeneity in the substrate wettability resulted in a lateral contribution to the droplet velocity over the course of the rebound. In the majority of the above numerical tests, the droplets had a size in the millimetre range and it impacted with the substrate at a velocity approaching some 1 m.s^{-1}. The rebound simulation of a micro-droplet impacting at a higher velocity attaining some 50 m.s^{-1} were also recently simulated [A31].

1.1.4 Direct numerical simulation of a liquid droplet interacting with a fluidic substrate

A large number of numerical advancements were suggested to study the coalescence of a liquid droplet with the fluidic substrate. Blanchette et al. [A32] used a ***binary fluid model*** to predict the partial and the full coalescence of a water droplet gently brought into contact with an air-water interface. Boyer et al. [A33] later developed a ***ternary fluid model*** to simulate the ascension of a gas droplet across a fluidic interface. The team could reproduce the entrainment of the heavier bottom fluid into the lighter upper fluid during the droplet motion across the interface. The bottom heavier fluid accumulated in the region downstream of the rising droplet. More recently, Feng et al. [A6] studied experimentally and numerically the rise of an air bubble towards an oil-water interface. As seen in Figure 5, the ternary fluid system consisted of a water droplet initially placed at the bottom of a water tank. On the water surface rested a thin oil film. The ratio of the bubble radius d_b to the thickness h of the oil film varied from approximately $d_b/h = 0.6$ to 2. Using a front-tracking method, the downward bouncing of the air droplet off the fluidic interface agreed remarkably well with the experimental data. The right diagram in Figure 5 shows the droplet velocity undulating from positive to negative values until it reaches a stable equilibrium position. Unlike the previous study performed by Boyer et al. [A33], the droplet here never entered the upper fluid. Conversely, it kept bouncing in the water until it reached an equilibrium position. The oscillating response of the bouncing droplet was comparable to that of a damped mass-spring system described in Eq. (1). The vertical droplet position described sinusoidal oscillations contained in an exponentially decaying envelope, thereby, stressing again the striking resemblance to the dynamics of a droplet bouncing off an elastic superhydrophobic substrate [A22, A23]. To the best of the candidate's knowledge, Feng et al. [A6] were one of the few who actually used a direct numerical simulation to study droplet rebound off a fluidic interface.

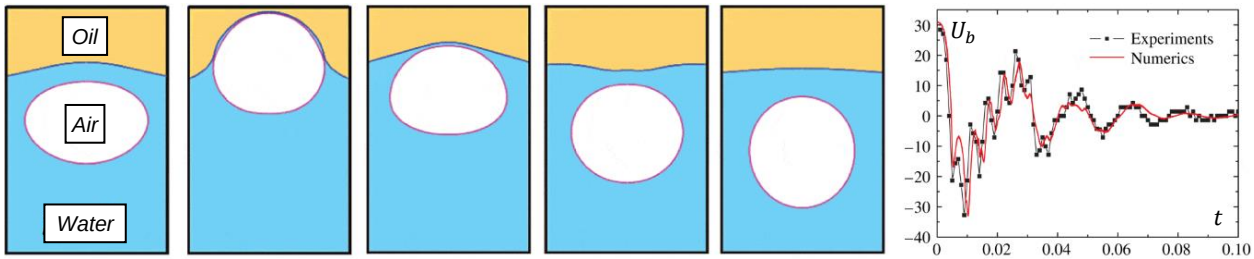

Fig. 5*: An air bubble rises towards an oil-water interface [A6]. The bouncing is illustrated on the right subfigure. The droplet velocity $U_b(t)$ undulates from positive to negative values until it reaches an equilibrium position. The oscillating response of this ternary system exhibits a striking resemblance to a damped mass-spring system in Eq. (1).*

Sadullah et al. [A11] recently developed a ternary fluid model and simulated the translation of a water droplet on a liquid-infused substrate using a lattice-Boltzmann method. The local deformation of the fluidic substrate at the three-phase contact point could be accurately predicted. Figure 6 shows the direct numerical simulation of a two-dimensional liquid droplet at rest on a liquid-infused surface. The droplet elongation is shown for increasing contact angles.

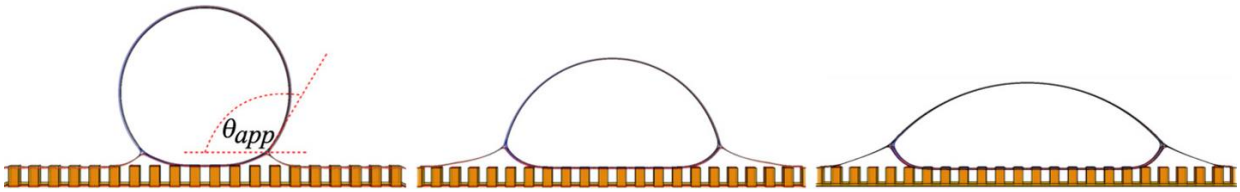

***Fig. 6**: Two-dimensional direct numerical simulation of a droplet at rest on a liquid-infused interface. Simulation are shown for increasing contact angles.*

1.1.5 Phase field theory to simulate droplet dynamics

The majority of the direct numerical simulations cited above were performed with a front tracking method [A32]. This method essentially relies on an indicator function constructed from the "known" position of the sharp interface [A34, A35]. With the continuous mathematical development and the increasing affordability of computational power, ***the phase field theory has gained popularity*** and started to be used for the direct numerical simulation of multiphase flow phenomena [A36, A37]. The phase field model makes use of an alternative order parameter, a so-called phase field $\psi(\mathbf{x}, t)$, to characterise the various fluid constituents, where $\mathbf{x}$ is the spatial coordinate and t the time. The phase field undergoes a rapid but smooth variation across the interfacial region. The simulation of the droplet rebound shown in Figure 4 was performed with a phase field model. The authors coupled a Cahn-Hilliard binary model with a Navier-Stokes solver [A28]. Borcia et al. [A38] also recently used a similar binary fluid model to simulate the "dancing" of liquid droplet on horizontally vibrating substrate. Direct numerical simulation based on the phase field theory were also reported for ternary flows [A11, A33, A39] and for systems made up of an arbitrary number of fluid phases [A40, A41].

1.1.6 Conclusions to the state of the art

The dynamics of droplet interacting with a solid hard substrate are now fairly well understood and models have reached a good level of maturity. Yet, many important questions on droplet interaction with a deformable substrate remain unanswered. The above literature has shown that the following gaps have not yet been bridged:

- A droplet interacting with a fluidic substrate exhibits rich dynamics, ***strongly reminiscent of those observed with a solid (visco)elastic substrate***. Only a few direct numerical simulations have so far been suggested to better understand the complex interaction of a fluid droplet with a fluidic substrate, be it a sliding or an impacting droplet.
- A droplet impacting with a fluidic substrate is a typical ternary fluid system and, as such, it can be accurately modelled with a phase field model. The large majority of the available direct numerical simulations ***were primarily intended to study the impact of a droplet with a hard substrate***. Very few simulations were performed to study the dynamics of a droplet impacting with a fluidic elastic substrate.
- Simulations have largely been applied to study the impact of a single droplet. ***Direct numerical simulations of multiple droplets impacting with an elastic substrate are scarce***. In the case of a hard substrate covered by thin liquid film, the wave propagation of the fluidic interface caused by a first droplet impact should generate a lateral contribution to the neighbouring impacting droplets. Such direct numerical simulations are missing in the literature.

1.2 Preliminary work

1.2.1 Growth and deterioration of a multi-layered particle substrate in a turbulent flow

The applicant has strong experimental and numerical expertise on the dynamic interaction of a multi-layered particle substrate with a turbulent airflow [B1-B4]. In a first study, the build-up of multi-layered particle substrate was studied in a pure deposition regime. A dilute concentration of micron-particles was injected upstream of an obstructed turbulent channel flow. The experiment was paused every hour and the height of air-granular interface of the substrate was measured using a laser scanner. The growth of the multi-layered particle substrate was then simulated using an in-house algorithm, which brought together a particle transport model, a direct numerical flow

simulation, and an in-house granular model based on self-organised criticality. Figure 7 shows the experimental and numerical evolution of the multilayer deposit as a function of time. The model predicted remarkably well the build-up of the multi-layered particle substrate in the cavity. The granular pile formation near vertical surfaces was accurately captured. In a second study, the particle remobilisation off multi-layered particle substrate was investigated.

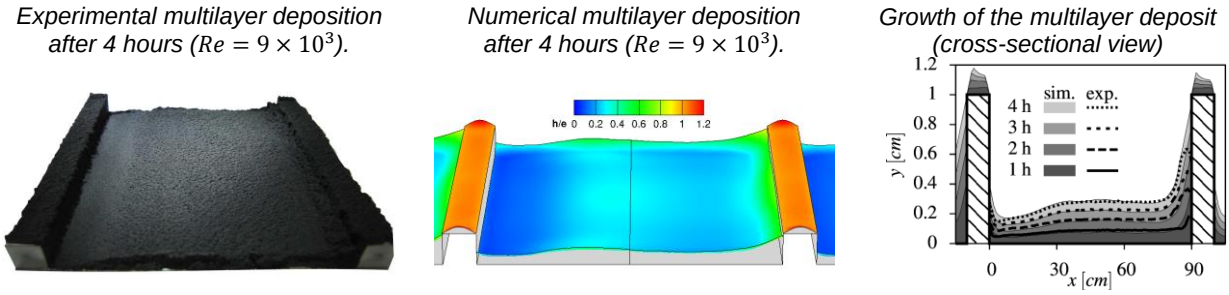

Fig. 7*: Growth of a multi-layered particle substrate in the deposition regime. By alternating steps of computational fluid dynamics to simulate the deposition and steps of granular mechanics to simulate the growth of the particle deposit, the formation of the multi-layered particle substrate could be simulated.*

1.2.2 Particle interaction with a fluidic substrate

The applicant has enjoyed over the last two years an advanced Marie-Curie training at the partner University of Kyoto, Japan, where he worked on the ***dynamic interaction of colloidal particles with a fluidic substrate***. A brief overview of the achieved experimental and numerical results is given below.

<u>*Experimental attachment:*</u> Using an in-house high-speed microscope immersed in water, the attachment of hydrophobic elongated particles to the surface of a stationary gas bubble was investigated [B5]. As illustrated in Figure 8, it was found that the type of attachment depended on the collision angle. Whenever the particle collided close to the upper pole of the bubble, a tangential alignment was observed. A collision 30° further down the bubble surface resulted in a radial attachment of the fibre with the fluidic interface. The contact angle of the glass particles at an air-water interface equated 60°. The experimental trajectories of the experimental attachments were then used to develop and validate a simulation model of reduced complexity, which delivered particle velocities and trajectories in excellent agreement with the experimental data.

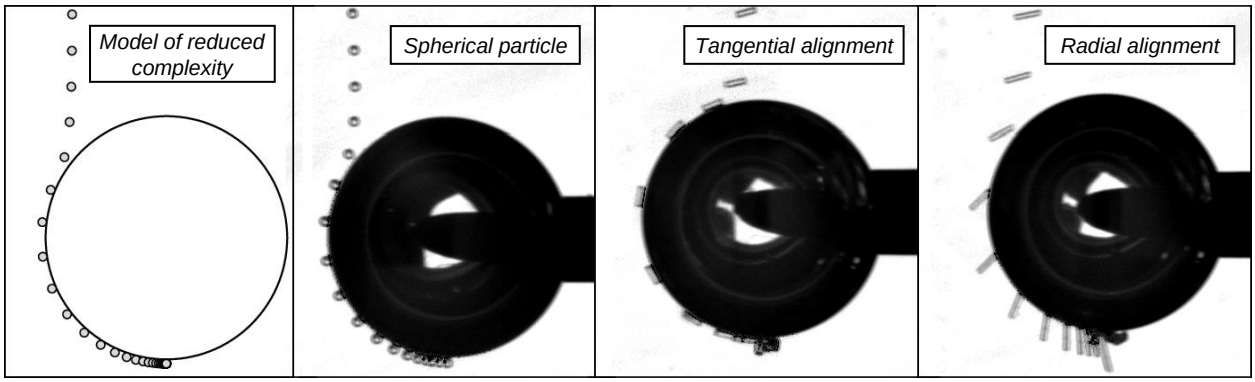

Fig. 8*: Attachment of spherical and elongated glass particles to the fluidic interface of a stationary air bubble immersed in water. Upon collision near the upstream pole of the gas bubble the major axis of the fibre aligns with the local bubble surface (tangential fibre alignment). If collision occurs at least 30° further downstream only the head of the fibre is in contact with the gas–liquid interface (radial fibre alignment).*

<u>*Fully resolved attachment model*</u>: In an attempt to further develop numerical tools which will find future applications in the recovery of mineral particles by rising bubbles, a direct numerical

simulation of particle dynamics at a fluidic interface was performed [B6-B8]. The applicant combined the “Smooth Profile Method”, originally developed at the Kyoto University for the direct numerical simulation of colloidal particles in monophasic fluids [A42], with a modified phase field model. The development of the Smooth Profile Method is now well documented and has found widespread applications ranging from the rheological behaviour of colloidal dispersions [A43] to the study of self-propelled microorganisms [A44]. This extended method, here termed the ***Extended Smooth Profile Method***, essentially involved the replacement of the particle-fluid boundary with a smoothly spreading interface. To this end, the smooth profile $\phi_{\mathrm{p}}(\mathbf{x},t)$, which transitioned from unity inside the colloidal region to zero in the outer region, was introduced. The total Eulerian fluid velocity field was decomposed as $\mathbf{u} = \phi_{\mathrm{p}}\mathbf{u}_{\mathrm{p}} + (1-\phi_{\mathrm{p}})\mathbf{u}_{\mathrm{AB}}$, where the term $\phi_{\mathrm{p}}\mathbf{u}_{\mathrm{p}} = \phi_{\mathrm{p}}[\mathbf{V}_{\mathrm{p}} + \boldsymbol{\Omega}_{\mathrm{p}} \times (\mathbf{x} - \mathbf{X}_{\mathrm{p}})]$ was the velocity field of the colloidal particle and the term $(1-\phi_{\mathrm{p}})\mathbf{u}_{\mathrm{AB}}$ the velocity field of the binary fluid. The Lagrangian fields $\mathbf{V}_{\mathrm{p}} = \mathrm{d}\mathbf{X}_{\mathrm{p}}/\mathrm{dt}$ and $\boldsymbol{\Omega}_{\mathrm{p}}$ were the translational and rotational particle velocities, respectively. The total fluid velocity was updated in time by solving a modified momentum equation of the form

$$\rho\left[\frac{\partial \mathbf{u}}{\partial t} + (\mathbf{u}\cdot\nabla)\mathbf{u}\right] = \nabla\cdot(-p\mathbf{I} + \boldsymbol{\sigma}_{\mathrm{v}}) + \rho\phi_{\mathrm{p}}\mathbf{f}_{\mathrm{p}} - \left(\psi\nabla\mu + \phi_{\mathrm{p}}\nabla\mu_{\mathrm{p}}\right), \tag{3}$$

where p was the pressure, $\boldsymbol{\sigma}_{\mathrm{v}}$ the viscous stress tensor, $\mathbf{f}_{\mathrm{p}}$ a penalty term enforcing the particle rigidity [A45], and $-\psi\nabla\mu - \phi_{\mathrm{p}}\nabla\mu_{\mathrm{p}}$ the capillary contribution. The separation of the binary fluid mixture into its two constituent fluid phases “A” and “B” was driven by the minimisation of a free energy $\mathcal{F}$, from which the two chemical potentials $\mu = \delta\mathcal{F}/\delta\psi$ and $\mu_{\mathrm{p}} = \delta\mathcal{F}/\delta\phi_{\mathrm{p}}$ were derived. To account for the deformation of the fluidic interface, the order parameter $\psi(\mathbf{x},t) = \phi_{\mathrm{A}} - \phi_{\mathrm{B}}$ was introduced where ϕ_{A} was the volume fraction of the fluid “A” and ϕ_{B} that of the fluid “B”. To compute the evolution of the gas-liquid interface, defined as the isosurface $\psi = 0$, the order parameter was updated in time according to the following modified Cahn-Hilliard equation

$$\frac{\partial\psi}{\partial t} + \nabla\cdot\left[\nabla\mathbf{u} + M\left(\mathbf{I} - \phi_{\mathrm{p}}\otimes\phi_{\mathrm{p}}\right)\nabla\mu\right] = 0. \tag{4}$$

The application of the Extended Smooth Profile Method to simulate the settling of a hydrophobic colloidal particle of arbitrary shape towards a fluidic interface is illustrated in Figure 9 for two Bond numbers. The Bond number $\mathrm{Bo} = |\rho_{\mathrm{A}} - \rho_{\mathrm{B}}|g\,r_{\mathrm{p}}^2/\gamma_{\mathrm{AB}}$ denotes the ratio of the gravitational force to the reference capillary force, where g is the gravitational acceleration, $\mathrm{r_p}$ the radius of a single bead, and γ_{AB} the surface tension.

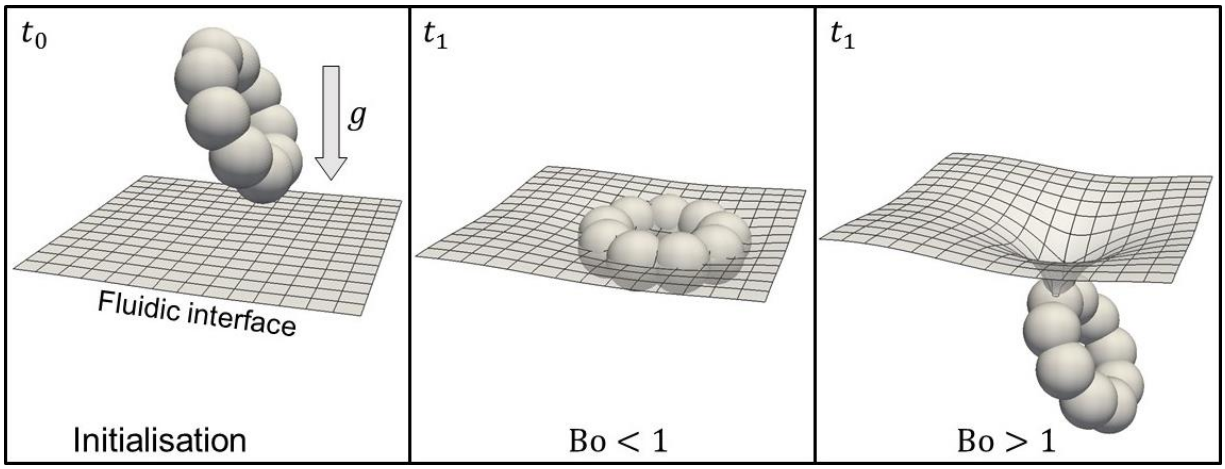

Fig. 9*: Dynamics of a three-dimensional torus-like hydrophobic particle settling towards a fluidic interface. The simulation snapshots are shown for two Bond numbers. A larger Bo generally results in a larger deformation of the fluidic interface until detachment eventually occurs.*

In line with previous experiments [A46, A47], for a Bond number $\mathrm{Bo} \ll 1$ the fluidic interface hold the colloidal particle with only little deformation. The rotation of the non-spherical colloid caused by the capillary torque [A48] was also captured. The torus-like particle smoothly rotated at the fluidic interface until a stable horizontal position was reached. With increasing Bond number, the assembly penetrated deeper into the bottom fluid phase. Exceeding a critical value caused the particle to eventually break away from the fluidic interface.

1.2.3 Example of a rising droplet across a colloidal swarm

The model was recently extended to study the three-dimensional interaction of multiple hydrophopic particles with a rising droplet [B8]. An extra gravity term was inserted into the momentum Eq. (3) so that the bubble could move upwards as a result of the buoyancy. Figure 10 shows a typical snapshot of the simulation. The work essentially involved the implementation of a Lennard-Jones potential, which avoided the non-physical overlapping of the colloidal particles. The smooth transition of the phase field $\psi(\mathbf{x}, t)$ from one phase to another is illustrated in the right subfigure.

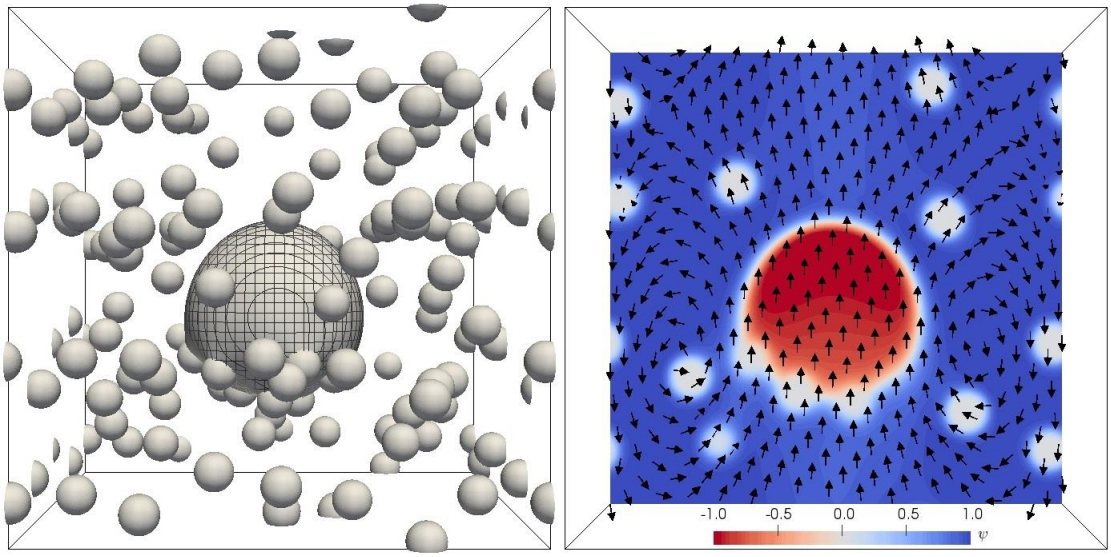

***Fig. 10**: Rising of a three-dimensional droplet across a particle cloud (left). The ψ-contour is also shown in the domain mid-section (right). The scalar field ψ, which is an indirect measure of the volume fraction, equates $\psi = 1$ in the ambient fluid, $\psi = -1$ in the fluid droplet, and $\psi = 0$ inside the colloid. The velocity vectors are shown in black.*

1.2.4 Elasto-capillary deformation of a fibre substrate

The candidate's recent preliminary work also includes the elasto-capillary deformation of an elastic substrate by a liquid droplet. In this work, the deformable fibre was constructed as a collection of overlapping three-dimensional beads. Each bead of the chain underwent stretching, bending and twisting interactions with its next neighbouring beads. The fibre decomposition into a flexible bead chain was inspired from a linear viscoelastic model [A49]. The stretching force, acting on the i-th bead of the chain, was modelled as

$$\mathbf{F}_i^S = -k_\mathrm{s}(|\mathbf{X}_{i+1} - \mathbf{X}_i| - 2\mathrm{r}_b)\,\mathbf{t}_i, \tag{5}$$

where k_s was the stretching modulus, $\mathbf{X}_i$ the position of the i-th bead, r_p the particle bead radius, and $\mathbf{t}_i = (\mathbf{X}_{i+1} - \mathbf{X}_i)/|\mathbf{X}_{i+1} - \mathbf{X}_i|$ a unit vector describing the local fibre direction. The bending and the torsion were implemented in a similar fashion. Figure 11 shows a situation, in which a deformable fibre partially wrapped the droplet initially at rest. Our preliminary results showed good agreement with literature data.

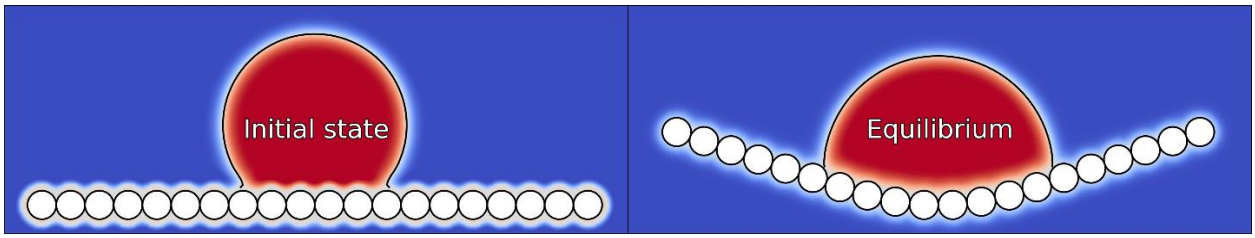

***Fig. 11**: Elasto-capillary bending of a flexible fibre substrate by a fluid droplet. The fibre was decomposed into a chain of spherical beads, which underwent stretching, bending and twisting interactions. The fluidic substrate and the two fluid-solid interfaces were replaced with smoothly spreading interfaces, in line with the Extended Smooth Profile Method.*

1.3 Intermediate conclusions on the preliminary works

- The applicant also has a strong experience in the fields of numerical and experimental two- and three-phase flows. ***A distinguished feature of the applicant's research lies in the interaction of non-spherical colloidal particles with a fluidic interface***. These preliminary works provide a favourable environment for the numerical investigation of liquid droplet interacting with a fluidic substrate.
- The applicant has a solid expertise in simulating substrate deformation caused by either hydrodynamic and/or capillary effects. The applicant recently extended his work to study the ***elasto-capillary deformation of a flexible substrate by a fluid droplet***. This test case matches the scope of this priority programme.
- The various numerical tools, which the applicant developed over the last years, reflect his strong involvement in the numerical modelling of complex multiphase flow phenomena. ***The applicant brought to fruition an in-house code for the direct numerical simulation of ternary flows,*** namely the transport colloidal particles in binary systems. The Extended Smooth Profile Method prepares well the ground for the unsteady simulation of impacting droplets with a fluidic substrate.

1.4 Project-related publications

1.4.1 Articles published by outlets with scientific quality assurance

[B1] Lecrivain, G., Rayan, R, et al., "Using quasi-DNS to investigate the deposition of elongated aerosol particles in a wavy channel flow", ***Computers & Fluids 124*** (2016), 78-85.
[B2] Barth T., Lecrivain, G., et al., "Particle deposition study in a horizontal turbulent duct flow using optical microscopy and particle size spectrometry", ***Journal of Aerosol Science 60*** (2013), 47-54.
[B3] Lecrivain, G., Sevan, D., et al., "Numerical simulation of multilayer deposition in an obstructed channel flow", ***Advanced Powder Technology 25*** (2014), 310-320.
[B4] Lecrivain, G., Barry, L., et al., "Three-dimensional simulation of multilayer particle deposition in an obstructed channel flow", ***Powder Technology 258*** (2014), 134-143.
[B5] Lecrivain, G., Petrucci, G., et al., "Attachment of solid elongated particles on the surface of a stationary gas bubble". ***International Journal of Multiphase Flow 71*** (2015), 83-93.
[B6] Lecrivain, G., Yamamoto, R., et al., "Direct numerical simulation of a particle attachment to an immersed bubble". ***Physics of Fluids 28*** (2016), 083301.
[B7] Lecrivain, G., Yamamoto, R., et al., "Direct numerical simulation of an arbitrarily shaped particle at a fluidic interface". ***Physical Review E 95*** (2017), 063107.
[B8] Lecrivain, G., Kotani, Y., et al., "Diffuse interface model to simulate the rise of a fluid droplet across a cloud of particles". ***Physical Review Fluids 3*** (2018), 094002.

2 Objectives and work programme

2.1 Anticipated total duration of the project

The project will last for three years and is anticipated to start on October 1st, 2019.

2.2 Objectives

The objective of this work is the development of a ternary fluid model for the direct numerical simulation model of droplet impact with a fluidic elastic interface. The applicant is here particularly interested in the simulation of droplet impact on a (A) flexible fluidic interface, and on (B) a hard solid substrate covered by a thin liquid film. In the longer run, this project will also look at the simulation of droplets impacting with an elastic gel-type substrate either dry or covered by a thin liquid film. The timeline of the three suggested work packages is shown in Figure 12. Note that the high-energy impact, prompting the droplet splashing, is here out of scope.

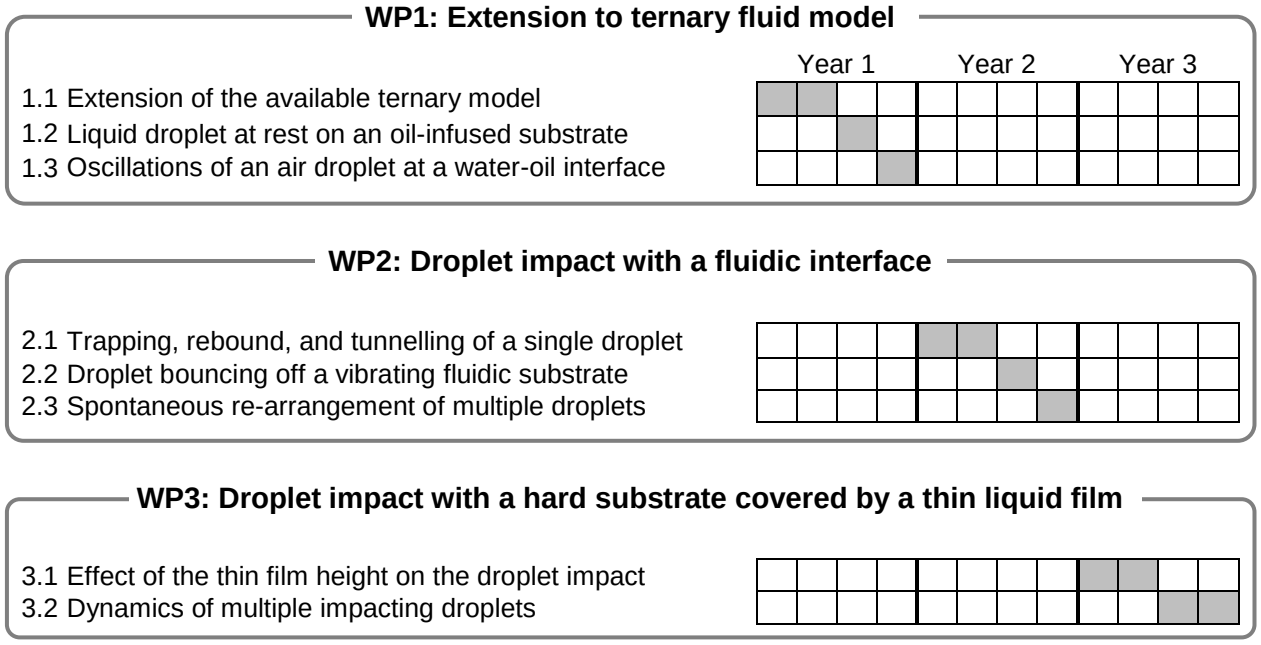

***Fig. 12**: Timeline of the suggested three work packages.*

2.3 Work programme incl. proposed research methods

Work Package 1: Extension to a ternary fluid model

Task 1.1: Extension to a ternary fluid model. The available ternary Fluid/Fluid/Solid Cahn-Hilliard model, recently developed by the applicant to study the attachment of solid particles to a fluidic interface, will here be advanced to simulate the dynamics of a liquid droplet interacting with a fluidic substrate. The numerical advancement will involve the modification of the free energy $\mathcal{F}(\phi_{\mathrm{A}}, \phi_{\mathrm{B}}, \phi_{\mathrm{C}})$, where $\phi_{\mathrm{A}}(\mathbf{x}, t)$ will be the volume fraction of the ambient fluid "A", $\phi_{\mathrm{B}}(\mathbf{x}, t)$ that of the second ambient fluid "B", and $\phi_{\mathrm{C}}(\mathbf{x}, t)$ that of the droplet liquid "C". The ternary phase system will be driven by the minimisation of a free energy, which will be the summation of a bulk term f_{b} with three additional interfacial components. In a similar fashion to the candidate's previous work, the total free energy will take the form

$$\mathcal{F} = \frac{k_{\mathrm{B}}\mathrm{T}_0}{\mathrm{v}_0}\int_{\mathcal{V}} \left\{ f_{\mathrm{b}}(\phi_{\mathrm{A}}, \phi_{\mathrm{B}}, \phi_{\mathrm{C}}) + \frac{\xi_{\mathrm{A}}^2}{2}|\nabla\phi_{\mathrm{A}}|^2 + \frac{\xi_{\mathrm{B}}^2}{2}|\nabla\phi_{\mathrm{B}}|^2 + \frac{\xi_{\mathrm{C}}^2}{2}|\nabla\phi_{\mathrm{C}}|^2 \right\} \mathrm{d}\mathbf{x} \tag{6}$$

where k_{B} is the Boltzmann constant, T_0 a reference temperature, v_0 a reference unit volume, and $\mathcal{V}$ the region of space occupied by the ternary system. The user-defined interfacial lengths ξ_{A}, ξ_{B}, and ξ_{C} will be introduced to control the surface energy, and hence to allow an exact definition of the contact angle at the three phase contact line. The bulk component f_{b} of the free energy density will have three global minima. A mathematically consistent expression for the bulk density $f_{\mathrm{b}}(\phi_{\mathrm{A}}, \phi_{\mathrm{B}}, \phi_{\mathrm{C}})$ will be implemented [A33, A41]. Figure 13 shows the plot of a consistent three-dimensional polynomial function

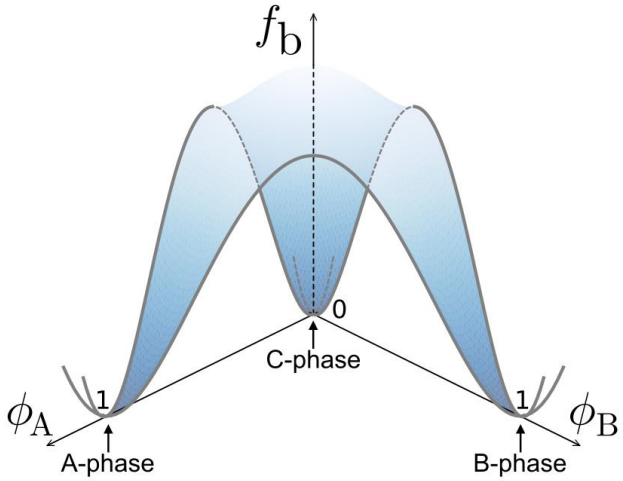

***Fig. 13**: The ternary mixture separates into its three immiscible fluid constituents A, B, and C. In the phase field theory, the separation is driven by the minimisation of the free energy, hence the three global minima. The present polynomial expression of the bulk free energy density $f_\mathrm{b}(\phi_\mathrm{A}, \phi_\mathrm{B}, \phi_\mathrm{C})$ is shown using the summation constraint $\phi_\mathrm{C} = 1 - \phi_\mathrm{A} - \phi_\mathrm{B}$. The function simplifies to the well-known double well function used in binary fluid studies.*

Similar to the advection Eq. (4), the three volume fractions $\phi_{i=\mathrm{A,B,C}}$ will be advanced in time as

$$\partial \phi_i / \partial t + \mathbf{u} \cdot \nabla \phi_i = \nabla^2 \mu_i \tag{7}$$

where $\mu_i = \delta \mathcal{F} / \delta \phi_i$ is the chemical potential. A Lagrangian multiplier will also be used to ensure the summation constraint $\phi_\mathrm{A} + \phi_\mathrm{B} + \phi_\mathrm{C} = 1$

Task 1.2: Liquid droplet at rest on an oil-infused substrate. The ternary Cahn-Hilliard model implemented in Task 1 will first be validated without the hydrodynamics in a two-dimensional and in a three-dimensional system. The model will be validated against known theoretical cases available in the literature. Benchmarks essentially describe the shape of a liquid droplet trapped between two immiscible fluids. To further stimulate the internal collaboration with partners involved in this priority programme, an additional validation will involve the simulation of a water droplet at rest on a oil-infused interface. Of particular interest will be the local deformation of the thin oil film near the three-phase contact line. A typical illustration of the substrate deformation into a ridge was shown in Figures 2 and 6. The numerical results will be compared with the experimental and simulation data made available by other groups involved in this priority programme.

- **Collaborations**: The experimental measurement of the deformed thin oil film near the three-phase contact line will be made available by S. Hardt, Technical University of Darmstadt. The experimental data will be used to validate the ternary fluid model for a liquid droplet lying at rest on an oil-infused substrate. Comparative simulations of a static liquid droplet resting on a thin oil-film will also be jointly performed with J. Harting, Forschungszentrum Jülich. The simulations will be done for increasing droplet affinities.

Task 1.3: Damped oscillations of an air droplet at a water-oil interface. The coupling between the ternary Cahn-Hilliard model and the hydrodynamic model will here be validated. This task will aim at reproducing the rise and the subsequent damped oscillation of an air droplet rising in water and eventually impacting with a thin oil film. An effective implementation of the momentum and of the Cahn-Hilliard equations will be essential to simulate flows with a density ratio of up to 1000. A 5$^{\mathrm{th}}$-order space discretisation WENO scheme for the advection terms, along with a 4$^{\mathrm{th}}$-order space discretisation combined with a Crank-Nicholson time discretisation for the biharmonic operators

$\nabla^4\phi_{i=\mathrm{A,B,C}}$ were recently implemented in the PETSC library for two-dimensional binary flows. Preliminary simulations showed excellent scalable properties on the high performance computing centre. Further effort will be necessary for efficient three-dimensional simulations. ***A dual grid system will be used. A grid with fine space resolution will be employed to solve the Cahn-Hilliard Eq. (6), while a coarser grid will be employed to solve the momentum and pressure equations***. A series of field interpolation will then be performed between the fine and the coarse grids [A36], hence speeding up the simulation quite substantially and, at the same time, avoiding the use of local mesh refinement across the interface. The simulation results will be compared to the numerical and experimental data previously performed on an air bubble rising in water and eventually bouncing off an oil-water interface. The damped oscillations off the interface will be captured with the combined phase-field/hydrodynamic model.

- **Collaboration**: The effective three-dimensional implementation of the hydrodynamic model will be incorporated into the existing binary fluid-structure interaction model in Eq. (5). The doctoral student of P. Lorenz, Leibniz – Institute of Surface Engineering, Leipzig, will enjoy a two-week training organised by the principal investigator. The training will aim at simulating the wrapping of a highly deformable thin elastic structure around an impacting water droplet. In this process, known as micro-origami, the thin structure will be modelled as a collection of spherical beads. The training will be a continuation of the preliminary work shown in Figure 11.

Work Package 2: Droplet impact with a fluidic interface

Task 2.1: Trapping, rebound, and tunnelling of a single droplet. In the present tasks the droplet impact with a fluidic interface under increasing Weber numbers will be studied numerically. Recent experimental observations on droplets impacting with a smectic film revealed remarkable dynamics [A5]. Depending on the impacting velocity, the droplet may either A) get trapped at the interface, B) keep bouncing off the interface until it reaches an equilibrium position, or c) tunnel through the interface. Droplet tunnelling indicated that the droplets broke away from the fluidic interface. These three modes depended on the impacting velocity. With a Weber number well below unity, trapping normally occurred. In the bouncing regime, droplet deformation could be quite significant. References [A3, A4] reported oblate-like deformation of the droplet with a height half of its initial diameter. Beyond a critical value, normally ranging from We=10 to 20 tunnelling occurred. A set of axisymmetric simulations will be performed. Figure 14 shows a schematic of the simulation. The Weber number will here be varied from 0.1 to 20. The upper interval limit of $\mathrm{We}_{\mathrm{max}}$ = 20 will be chosen because tunnelling normally occurs beyond a critical value lying in the range We_{c} = 10 to 16. The results from this set of direct numerical simulations will deliver a phase diagram, which will characterise the following anticipated modes, namely trapping, droplet rebound, and tunnelling. To capture the droplet encapsulation, the thin film will be modelled differently. The fluidic substrate will be modelled as thin liquid film “B” separating the two ambient fluids “A”. The height of the fluidic membrane will be artificially extended to allow a smooth transition of the phase fields.

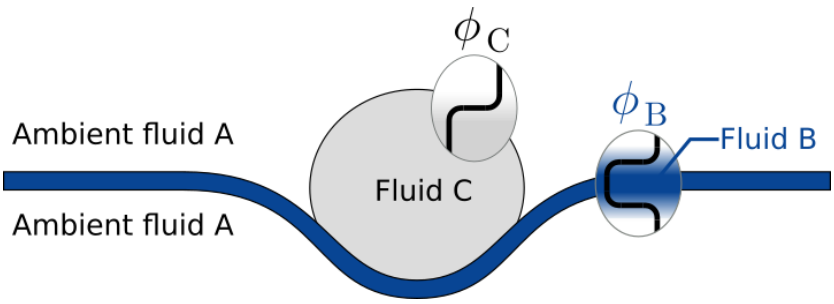

Fig. 14*: Schematic of the numerical set-up, which will be used to simulate the droplet impact with a smectic film and with a soap surfactant film. Modelling the fluidic membrane as an artificially thick film will allow the simulation of the droplet encapsulation, i.e. the trapping mode. Fluid C is normally composed of water and glycerol.*

Note, that a freestanding smectic/soap film is a thin membrane separating two air phases. The hydrodynamics are not exactly identical to those observed with a fluidic interface separating by two immiscible fluids, such as an air-oil interface. Yet, the dominant effect to be investigated here is the restoring capillary force exerted by the fluidic interface onto the droplet. The ternary fluid field will reproduce the droplet dynamics caused by the smectic membrane, such as the droplet rebound and its encapsulation in the film.

- **Collaboration***:* The simulated three modes are compared with the experimental investigations performed by R. Stannarius, University of Magdeburg. Further simulations will extend the state of the art by looking at the impact of a droplet with two smectic films placed on top of each other. A droplet tunnelling across the first smectic film might not possess sufficient energy to cross the second film below.

Task 2.2: Droplet bouncing off a vibrating fluidic substrate. The developed model will be employed to simulate the dynamics of a single droplet impacting with a vertically vibrating fluidic substrate. The simulation will be performed with a Weber number close to We = 2 to 5. This numerical experiment will mimic the droplet rebound either on a vibrating freestanding soap film, or on a vibrating liquid bath. In the latter, the bath container is normally brought into vertical vibration. An axisymmetric direct numerical simulation will here be performed. The vibration of the substrate will be enforced at the domain boundary by prescribing a sine wave function of the form

$$\phi_{\mathrm{A}}\left(y_{\mathrm{boundary}}, t\right) = \frac{1}{2}\left\{1 + \tanh\left[\frac{y_0 + \lambda\cos(\omega t)}{\xi_{\mathrm{AB}}}\right]\right\}, \tag{8}$$

where λ is the oscillation amplitude, ω the frequency, and ξ_{AB} the interfacial length associated with the A/B interface. In the absence of oscillation, i.e. $\lambda = 0$, the above equation simplifies to the exact mathematical solution located at the minima $\delta\mathcal{F}/\delta\phi_{\mathrm{A}} = 0$ depicted in Figure 13. Based on previous experimental works [A3], the vibration frequency will be varied in the range $10\mathrm{Hz} < 2\pi/\omega < 50\mathrm{Hz}$. Note that the response time of a 1 mm water droplet in air roughly equates $\tau_{\mathrm{droplet}} = \rho_{\mathrm{liquid}} d_{\mathrm{droplet}}^2/(18\rho_{\mathrm{air}}\mu_{\mathrm{air}}) \approx 3\mathrm{s}$, a value much greater than the oscillation period set in Eq. (8). The discretisation time step of the simulation will hence be adequate to capture the dynamics of the system with a reasonable computational cost.

- **Collaboration***:* The doctoral student will conduct a measurement campaign at the partner's institution (Leibniz-Institut für Polymerforschung, Dresden) on the impact of single and multiple droplets with a vibrating freestanding surfactant film. G. Auernhammer will provide access and support in performing the experiments, and in processing and analysing the data.

Task 2.3: Spontaneous re-arrangement of multiple droplets. A single droplet bouncing off a vertically oscillating fluidic substrate ideally moves up and down. This is no longer true in the presence of multiple droplets. A first oscillating droplet generates a deformation wave, which propagates along the surface of the fluidic substrate. As a result, a lateral force is exerted by the deforming substrate onto the neighbouring oscillating droplets. This new horizontal contribution to the droplet velocities gives rise to remarkable dynamics. The orbiting motion of droplets or even their spontaneous re-arrangement into a self-assembled structure have been reported experimentally [A50]. An example of self-organised droplet re-arrangement on a vibrating oil bath is illustrated in Figure 15. This task will involve the direct numerical simulation of 3, 4, and 5 droplets impacting with a vertically vibrating fluidic substrate. The simulations will be performed in two- and three-dimensional domains with periodicity enforced on the lateral sides of the domain to avoid the undesirable effect of the walls on the droplet trajectories.

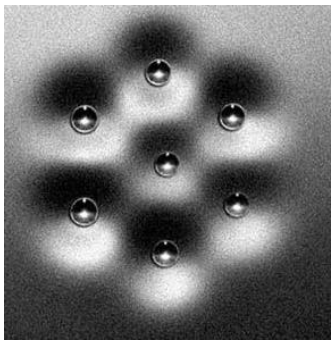

Fig. 15*: Seven droplets spontaneously rearrange into a self-assembled structure with a crystalline triangular lattice [A7]. When placed on a vertically oscillating fluidic substrate, the liquid droplet bounce for an unlimited time. A thin lubricating air layer between the impacting droplet and the substrate fluidic forms and prevents the coalescence with the substrate. This lubricating air layer is much smaller than the typical simulation grid size. In the present numerical tests, it will be modelled by using an apparent contact angle. The droplet will have a stronger affinity to air.*

Work package 3: Droplet impact with a hard substrate covered by a thin liquid film
Task 3.1: Effect of the film height on droplet impact. The ternary fluid model will here be employed to simulate a single droplet impinging on a hard substrate covered by a thin liquid film. Experimental measurements do not always provide all details of the impact since it happens within a short time period. In this task, a water droplet will impact with a hard substrate covered by a thin oil film. Figure 16 shows, for instance, the complex dynamics of a solid particle impacting with a thin oil film. In this example, the particle had a diameter of 1.7 mm and the oil film had a height of about 0.4 mm.

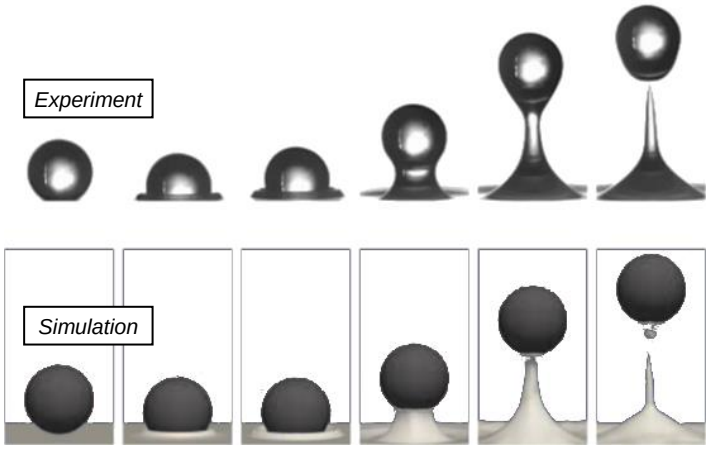

Fig. 16*: Sequence of images showing the formation of liquid bridge following the impact of hard spherical particle with a solid substrate covered with a thin oil film [A51]. The non-deformable particles hits the substrate with a velocity of 1.13 m/s. The simulation was performed with a Volume-of-Fluid method. The interface reconstruction algorithm was based on a piecewise linear interface calculation.*

A set of simulations will here be performed with a liquid droplet impacting with a thin film representing a second non-immiscible liquid, such as oil. The ratio of the droplet diameter to the height of the thin liquid film will be varied from h/d_b = 0.1 to 0.5. This ratio will correspond to that of a droplet at rest on an oil-infused interface [A10, A11]. Similar ratios were also reported for micro-droplets at rest on thin elastomer films [A1]. The restitution coefficient will be numerically derived as a function of the liquid film height. The deformation of the droplet will also be investigated for increasing Weber numbers ranging from We = 0.1 to 2. The oscillations will be compared to those simulated on a hard solid substrate.

- **Collaborations***:* The rebound of a single droplet off the thin oil film will also be studied experimentally by K. Harth, Magdeburg University. The predicted droplet deformation along with the damped oscillating behaviour of the bouncing droplet will be compared to the experimental data. A benchmark numerical study will also be performed together with R. Borcia, Brandenburg University of Technology Cottbus-Senftenberg. The benchmark will compare the particle restitution coefficient as a function of the height of the thin liquid film.

Task 3.2: Dynamics of multiple impacting droplets. The impact of multiple droplets with a thin liquid film will here be investigated numerically. As will be the case with the freestanding film simulation, 3, 4 and 5 droplets will be released from an altitude higher than that of the liquid film. The height of the thin liquid film will be set to h/d_b = 0.1. This low value will avoid a fast damping of the droplet velocity. The Weber number will vary from from We = 0.1 to 2. The effect of the wave propagation of the fluidic interface and its contribution to the lateral motion of the neighbouring droplets will be studied. The simulations will be performed in two- and three-dimensional domains with periodicity enforced on the lateral sides.

- **Collaboration***:* The dynamics of a pair of impacting droplets will be compared with the numerical results from the team composed of U. Thiele, Münster University, and J. Snoeijer, University of Twente. The two partners conduct experiment, simulation and theoretical work on droplet ensembles.

2.4 Data handling

The results will be published in high-ranking journals. Journal candidates are, but not limited to, Journal of Fluid Mechanics, Physics of Fluids, Physical Review Fluids, and Journal of Computational Physics. The experimental and numerical raw data will also be stored in a central data repository available at HZDR. The authors will make them broadly available to the scientific community, thereby ensuring a sustainable dissemination of the results.

2.5 Other information

Once a year, the HZDR and the Technical University of Dresden join the “Dresdener Lange Nacht der Wissenschaften” which translates to “Long Night of Sciences in Dresden”. All laboratories open their doors to the public from 6 pm until 1 am. The applicant will contribute to this event by preparing specific activities on droplet impact with a fluidic substrate, which will arouse public interest. A small facility will showcase the droplet oscillating and eventually rearranging into self-assemblies. The oscillations will be made tuneable by the public to change from the rebound regime to splashing regime occurring at higher impact velocities. Complementary simulations will be showed on monitors to further spark the interest of the public.

2.6 Descriptions of proposed investigations involving experiments on humans, human materials or animals as well as dual use research of concern

Not applicable

2.7 Information on scientific and financial involvement of international cooperation partners

Not applicable.

3 Bibliography

[A1] Pericet-Camara, R., Auernhammer, G.K.*, et al.*, "Solid-supported thin elastomer films deformed by microdrops", *Soft Matter 5* (2009), 3611-3617.
[A2] Gilet, T. and Bush, J.W.M., "Droplets bouncing on a wet, inclined surface", *Physics of Fluids 24* (2012), 122103.
[A3] Fell, D., Sokuler, M.*, et al.*, "Drop impact on surfactant films and solutions", *Colloid and Polymer Science 291* (2013), 1963-1976.
[A4] Gilet, T. and Bush, J.W.M., "The fluid trampoline: droplets bouncing on a soap film", *Journal of Fluid Mechanics 625* (2009), 167-203.
[A5] Dolle, S. and Stannarius, R., "Microdroplets Impinging on Freely Suspended Smectic Films: Three Impact Regimes", *Langmuir 31* (2015), 6479-6486.
[A6] Feng, J., Muradoglu, M.*, et al.*, "Dynamics of a bubble bouncing at a liquid/liquid/gas interface", *Journal of Fluid Mechanics 807* (2016), 324-352.
[A7] Harris, D.M. and Bush, J.W.M., "The pilot-wave dynamics of walking droplets", *Physics of Fluids 25* (2013),
[A8] Quere, D., "Non-sticking drops", *Reports on Progress in Physics 68* (2005), 2495-2532.
[A9] Tanner, L.H., "The spreading of silicone oil drops on horizontal surfaces", *Journal of Physics D: Applied Physics 12* (1979), 1473.
[A10] Keiser, A., Keiser, L.*, et al.*, "Drop friction on liquid-infused materials", *Soft Matter 13* (2017), 6981-6987.
[A11] Sadullah, M.S., Semprebon, C.*, et al.*, "Drop Dynamics on Liquid-Infused Surfaces: The Role of the Lubricant Ridge", *Langmuir 34* (2018), 8112-8118.
[A12] Shirtcliffe, N.J., McHale, G.*, et al.*, "Superhydrophobic copper tubes with possible flow enhancement and drag reduction", *ACS Appl Mater Interfaces 1* (2009), 1316-1323.

[A13]Roman, B. and Bico, J., "Elasto-capillarity: deforming an elastic structure with a liquid droplet", *J Phys Condens Matter 22* (2010), 493101.
[A14]Shanahan, M.E.R. and Carre, A., "Viscoelastic Dissipation in Wetting and Adhesion Phenomena", *Langmuir 11* (1995), 1396-1402.
[A15]Karpitschka, S., Das, S.*, et al.*, "Droplets move over viscoelastic substrates by surfing a ridge", *Nat Commun 6* (2015), 7891.
[A16]Mangili, S., Antonini, C.*, et al.*, "Understanding the drop impact phenomenon on soft PDMS substrates", *Soft Matter 8* (2012), 10045-10054.
[A17]Chen, L., Bonaccurso, E.*, et al.*, "Droplet impact on soft viscoelastic surfaces", *Phys Rev E 94* (2016), 063117.
[A18]Weisensee, P.B., Tian, J.*, et al.*, "Water droplet impact on elastic superhydrophobic surfaces", *Sci Rep 6* (2016), 30328.
[A19]Damak, M. and Varanasi, K., "Expansion and retraction dynamics in drop-on-drop impacts on nonwetting surfaces", *Physical Review Fluids 3* (2018), 093602.
[A20]Courbin, L. and Stone, H.A., "Impact, puncturing, and the self-healing of soap films", *Physics of Fluids 18* (2006), 091105.
[A21]Gilet, T. and Bush, J.W., "Chaotic bouncing of a droplet on a soap film", *Phys Rev Lett 102* (2009), 014501.
[A22]Vasileiou, T., Gerber, J.*, et al.*, "Superhydrophobicity enhancement through substrate flexibility", *Proceedings of the National Academy of Sciences of the United States of America 113* (2016), 13307-13312.
[A23]Kim, J.H., Rothstein, J.P.*, et al.*, "Dynamics of a flexible superhydrophobic surface during a drop impact", *Physics of Fluids 30* (2018), 072102.
[A24]PasandidehFard, M., Qiao, Y.M.*, et al.*, "Capillary effects during droplet impact on a solid surface", *Physics of Fluids 8* (1996), 650-659.
[A25]Yarin, A.L., "Drop impact dynamics: Splashing, spreading, receding, bouncing...", *Annual Review of Fluid Mechanics 38* (2006), 159-192.
[A26]Lunkad, S.F., Buwa, V.V.*, et al.*, "Numerical simulations of drop impact and spreading on horizontal and inclined surfaces", *Chemical Engineering Science 62* (2007), 7214-7224.
[A27]Tan, H., "Numerical study on splashing of high-speed microdroplet impact on dry microstructured surfaces", *Computers & Fluids 154* (2017), 142-166.
[A28]Fink, V., Cai, X.*, et al.*, "Drop bouncing by micro-grooves", *International Journal of Heat and Fluid Flow 70* (2018), 271-278.
[A29]Parizi, H.B., Rosenzweig, L.*, et al.*, "Numerical simulation of droplet impact on patterned surfaces", *Journal of Thermal Spray Technology 16* (2007), 713-721.
[A30]Raman, K.A., Jaiman, R.K.*, et al.*, "Lattice Boltzmann simulations of droplet impact onto surfaces with varying wettabilities", *International Journal of Heat and Mass Transfer 95* (2016), 336-354.
[A31]Visser, C.W., Frommhold, P.E.*, et al.*, "Dynamics of high-speed micro-drop impact: numerical simulations and experiments at frame-to-frame times below 100 ns", *Soft Matter 11* (2015), 1708-1722.
[A32]Blanchette, F. and Bigioni, T.P., "Partial coalescence of drops at liquid interfaces", *Nature Physics 2* (2006), 254-257.
[A33]Boyer, F., Lapuerta, C.*, et al.*, "Cahn Hilliard Navier–Stokes Model for the Simulation of Three-Phase Flows", *Transport in Porous Media* (2010), 463.
[A34]Anderson, D.M., McFadden, G.B.*, et al.*, "Diffuse-interface methods in fluid mechanics", *Annual Review of Fluid Mechanics 30* (1998), 139-165.
[A35]Unverdi, S.O. and Tryggvason, G., "A Front-Tracking Method for Viscous, Incompressible, Multi-Fluid Flows", *Journal of Computational Physics 100* (1992), 25-37.
[A36]Ding, H., Spelt, P.D.M.*, et al.*, "Diffuse interface model for incompressible two-phase flows with large density ratios", *Journal of Computational Physics 226* (2007), 2078-2095.
[A37]Aland, S. and Chen, F., "An efficient and energy stable scheme for a phase-field model for the moving contact line problem", *International Journal for Numerical Methods in Fluids 81* (2015),
[A38]Borcia, R., Borcia, I.D.*, et al.*, "Dancing drops over vibrating substrates", *European Physical Journal-Special Topics 226* (2017), 1297-1306.
[A39]Zhang, C.Y., Ding, H.*, et al.*, "Diffuse interface simulation of ternary fluids in contact with solid", *Journal of Computational Physics 309* (2016), 37-51.
[A40]Dong, S., "An efficient algorithm for incompressible N-phase flows", *Journal of Computational Physics 276* (2014), 691-728.
[A41]Kim, J., "A generalized continuous surface tension force formulation for phase-field models for multi-component immiscible fluid flows", *Computer Methods in Applied Mechanics and Engineering 198* (2009), 3105-3112.
[A42]Nakayama, Y. and Yamamoto, R., "Simulation method to resolve hydrodynamic interactions in colloidal dispersions", *Physical Review E 71* (2005), 036707.
[A43]Molina, J.J., Otomura, K.*, et al.*, "Rheological evaluation of colloidal dispersions using the smoothed profile method: formulation and applications", *Journal of Fluid Mechanics 792* (2016), 590-619.
[A44]Oyama, N., Molina, J.J.*, et al.*, "Purely hydrodynamic origin for swarming of swimming particles", *Physical Review E 93* (2016),
[A45]Nakayama, Y. and Yamamoto, R., "Simulation method to resolve hydrodynamic interactions in colloidal dispersions", *Physical Review E 71* (2005),
[A46]Duprat, C., Protiere, S.*, et al.*, "Wetting of flexible fibre arrays", *Nature 482* (2012), 510-513.
[A47]Stratford, K., Adhikari, R.*, et al.*, "Lattice Boltzmann for binary fluids with suspended colloids", *Journal of Statistical Physics 121* (2005), 163-178.
[A48]Davies, G.B., Kruger, T.*, et al.*, "Interface deformations affect the orientation transition of magnetic ellipsoidal particles adsorbed at fluid-fluid interfaces", *Soft Matter 10* (2014), 6742-6748.

[A49]Kabanemi, K.K. and Hétu, J.-F., "Effects of bending and torsion rigidity on deformation and breakage of flexible fibers: A direct simulation study", *The Journal of Chemical Physics 136* (2012), 074903.
[A50]Protiere, S., Boudaoud, A.*, et al.*, "Particle-wave association on a fluid interface", *Journal of Fluid Mechanics 554* (2006), 85-108.
[A51]Tang, Y.B., B.; Heinrich, S.; Deen, N.G.; Kuipers, J.A.M., "Direct numerical simulations of particle collisions on a wet surface", *8th International Granulation Workshop, Sheffield, UK* (2017)

4 Requested modules/funds

4.1 Basic Module

4.1.1 Funding for Staff

Substantial numerical development is needed for successful completion of the project. The candidate applies for 75% of a full-time Ph.D. position for a period of three years to conduct the numerical work. Each year, a master's student will support the work. Two of the 6-month internships will be funded by the HZDR directly. Only one "Studentische Hilfskraft" is presently applied for. For a period of six months, it amounts to (9.50 €/hour) x (19 hours/week) x (26 weeks) = 4693 €.

75% of a fulltime Ph.D. position for a period of three years	**TV-L 13**
One "Studentische Hilfskraft" for a period of 6-months	**4693 €**
Two master's students for a period of 6-months (funded by HZDR)	**0 €**

4.1.2 Direct Project Costs

4.1.2.1 Equipment up to Euro 10,000, Software and Consumables

The Ph.D. student will perform an experimental measurement campaign at the partner's institution Leibniz-Institut für Polymer-Forschung in Dresden. Consumables will be necessary to measure the trajectories of the droplets impacting with a freestanding surfactant film.

Consumables	**1000 €**

4.1.2.2 Travel Expenses

The results will be presented at conferences on a yearly basis. Participation from the principal investigator and from the Ph.D. student to the yearly meeting of the priority programme will also be considered. Discussions with other researchers will improve the scientific quality of the work. Participation to two national conferences in Year 1 and Year 2 are expected. A contribution will be submitted to the International Conference on Multiphase Flow in Year 3.

Contributions to conferences and SPP meetings	**5000 €**

4.1.2.3 **Visiting Researchers** (excluding Mercator Fellows)

Not applicable.

4.1.2.4 Expenses for Laboratory Animals

Not applicable.

4.1.2.5 Other Costs

Not applicable.

4.1.2.6 Project-related publication expenses

750 € a year will be allocated to project-related publication expenses. It will amount to a total of 2,250 Euros for a project duration of 3 years. One article will be published as open access in a high-ranking journal to ensure a greater dissemination of the work.

Project-related publication expenses	**2250 €**

4.1.3 Instrumentation

4.1.3.1 Equipment exceeding Euro 10,000

Not applicable.

4.1.3.2 Major Instrumentation exceeding Euro 50,000
Not applicable.

4.2 Module Temporary Position for Principle Investigator
Not applicable.

4.3 Module Replacement Funding
Not applicable.

4.4 Module Temporary Clinician Substitute
Not applicable.

4.5 Module Mercator Fellows
Not applicable.

4.6 Module Workshop Funding
Not applicable.

4.7 Module Public Relations Funding
Not applicable.

5 Project requirements
5.1 Employment status information
The candidate has a permanent employment tenure since January 2018.

5.2 First-time proposal data
Not applicable

5.3 Composition of the project group

Scientist	*Funding*	*Expertise*
• Prof. Uwe Hampel	Funded by the Institution	Measurement techniques for multiphase flows
• Prof. Kerstin Eckert	Funded by the Institution	Transport processes at fluidic interfaces
• Dr. Dirk Lucas	Funded by the Institution	Multiphase computational fluid dynamics

5.4 Cooperation with other researchers
5.4.1 Researchers with whom you have agreed to cooperate on this project
The collaborations mentioned in the above work package descriptions along with some external contributors, intended to increase the visibility of this priority programme, are summarised as follows:

Work Package 1: Extension to ternary fluid model

- ***Prof. Steffen Hardt***, Technical University of Darmstadt. The cooperation will involve the investigation of liquid droplet at rest on a lubricant-infused surface. Using the ternary phase field model, the local deformation of the thin oil film near the three-phase contact line will be simulated and compared to experimental data.
- ***Prof. Jens Harting,*** Forschungszentrum Jülich. The cooperation will involve the joint simulation of a liquid droplet at rest on a thin oil-film. The deformation of the liquid film near the three-phase contact line will compared. The simulations will be performed for increasing droplet affinities.
- ***Dr. Pierre Lorenz,*** Leibniz – Institute of Surface Engineering, Leipzig. The cooperation will involve the wrapping of an elastic structure by a falling liquid droplet. The candidate will train the guest Ph.D. student for a period of two weeks. In line with the candidate's preliminary work, the thin elastic three-dimensional structure will be modelled as a collection of bonded spherical beads.

Work package 2:

- ***Prof. Ralf Stannarius***, University of Magdeburg. The cooperation will involve the investigation of droplet impact with a free-standing smectic film. The trapping, rebound, and the tunnelling of the droplet will be compared with the simulation data.

- ***Dr. Günter K. Auernhammer***, Leibniz-Institut für Polymer-Forschung, Dresden. The Ph.D. student will perform an experimental measurement campaign on the impact of multiple droplets with a vibrating freestanding surfactant film.

Work package 3:

- ***Dr. Kirsten Harth,*** University Magdeburg. The cooperation will involve the investigation of droplet impact with a solid substrate covered by a thin liquid film. The predicted droplet deformation along with the droplet restitution coefficient will be compared to experimental data.
- ***Dr. Rodica Borcia***, Brandenburg University of Technology Cottbus-Senftenberg. The collaboration will lead to a numerical benchmark study on droplet impact with a hard substrate covered by a thin liquid film.
- ***Prof. Uwe Thiele,*** University of Münster and ***Prof. Jacco Snoeijer,*** University of Twente. The cooperation will involve a numerical comparison. The trajectories a pair of impacting droplets on an elastic substrate will be compared.

External collaborations:

- ***Prof. Kerstin Eckert*** and ***Prof. Uwe Hampel***, both from the Technical University of Dresden. They will be the university co-supervisors of the Ph.D student. They are renowned experts in the field of transport processes at fluidic interface and in multiphase flows.

5.4.2 Researchers with whom you have collaborated scientifically within the past three years

The applicant has been collaborating in the last three years with Prof. Uwe Hampel (HZDR und TU Dresden, 6 papers), with Prof. Ryoichi Yamamoto and Prof. Takashi Taniguchi (Kyoto University, 4 papers), with Prof. Jochen Fröhlich (TU Dresden, 1 patent), and with Prof. Xu Cheng (KIT, 1 paper).

5.5 Scientific equipment

A high performance-computing centre is available for performing the direct numerical simulation of droplet impacts. The HZDR operates three Linux clusters capable of running large-scale computational calculations.

5.6 Project-relevant cooperation with commercial enterprises

Not applicable

5.7 Project-relevant participation in commercial enterprises

Not applicable

6 Additional information

The present research proposal has not been submitted elsewhere, in whole or in part. The scientific director of the Helmholtz-Zentrum Dresden-Rossendorf, Prof. Dr. R. Sauerbrey, has approved the present proposal.

Grégory Lécrivain

Helmholtz-Zentrum Dresden-Rossendorf
Institut für Fluiddynamik
Bautzner Landstraße 400
01328 Dresden, Deutschland
☎ *+49 351 260 3768*
FAX *+49 351 260 13768*
✉ *g.lecrivain@hzdr.de*

Research experience

2017-2018 **Parental leave**, *Reduced working hours*

2016–2017 **Helmholtz-Zentrum Dresden-Rossendorf**, *Germany*, Marie-Curie fellowship
- Experimental investigation of particle attachment to an immersed gas bubble

2014–2016 **Kyoto University**, *Japan*, Marie-Curie fellowship
- Direct numerical simulation of particle transport at fluidic interfaces

2010–2014 **Helmholtz-Zentrum Dresden-Rossendorf**, *German*, Post-doctoral position
- Experimental investigation of particle deposition and remobilisation in turbulent air flows
- Direct numerical simulation of aerosol particle transport in turbulent flows

2009–2010 **Technical University Dresden**, *Germany*, Post-doctoral position
- Industry project aimed at optimising the shapes of external components sitting on high-speed vehicles

Education

2005–2009 **Manchester Metropolitan University**, *England*, Ph.D. studies
- Using reverse engineering and computational fluid dynamics to improve the performance of complex three-dimensional bodies interacting with a fluid flow

2002–2005 **Art et Métier ParisTech**, *France*, Master's studies
- Distinctive element of the French higher education system, which recruits their students with a selective procedure

2000–2002 **Preparatory class**, *France*
- Preparation for the competitive examination to French engineering schools, known as Grandes Ecoles

2000 **Baccalauréat**, *France*

Languages

German	Fluent
English	Fluent
French	Mother tongue
Japanese	Conversant

Selected publications

- Lecrivain G., Kotani, Y., Yamamoto R., Hampel U., and Taniguchi T. (2018), A diffuse interface model to simulate the rise of a fluid droplet across a cloud of particles, ***Physical Review Fluids 3***, 094002

- Lecrivain G., Yamamoto R., Hampel U., and Taniguchi T. (2017), Direct numerical simulation of an arbitrarily shaped particle at a fluidic interface, ***Physical Review E 95***, 063107
- Lecrivain G., Yamamoto R., Hampel U., and Taniguchi T. (2016), Direct numerical simulation of a particle attachment to an immersed bubble, ***Physics of Fluids 28***, 083301
- Lecrivain G., Rayan R., Hurtado A., and Hampel, U. (2016), Using quasi-DNS to investigate the deposition of elongated aerosol particles in a wavy channel flow, ***Computers & Fluids 124***, p. 78-85
- Lecrivain G., Petrucci G., Rudolph M., Hampel U., and Yamamoto R. (2015), Attachment of solid elongated particles on a gas bubble surface, ***International Journal of Multiphase Flow 71***, p. 83-93
- Lecrivain G., Vitsas A., Boudouvis A.G., and Hampel U. (2014), Simulation of multilayer particle resuspension in an obstructed channel flow, ***Powder Technology 263***, p. 142-150.
- Lecrivain G., Barry L., and Hampel U. (2014), Three-dimensional simulation of multilayer par-ticle deposition in an obstructed channel flow, ***Powder Technology 258***, p. 134-143
- Lecrivain G., Drapeau-Martin S., Barth T., and Hampel U. (2014). Numerical simulation of multilayer deposition in an obstructed channel flow, ***Advanced Powder Technology 25***, p. 310-320
- Barth T., Lecrivain G., and Hampel U. (2013), Particle deposition study in a horizontal turbulent duct flow using optical microscopy and particle size spectrometry, ***Journal of Aerosol Science 60***, p. 47-54
- Lecrivain G. and Hampel U. (2012), Influence of the Lagrangian integral time scale estimation in the near wall region on particle deposition, ***ASME Journal of Fluids Engineering 134***, p. 1-6

Patent

- Schönherr, H.S., Steinike, D., Rüdiger, F., Lecrivain, G., Fröhlich, J., Camera outdoor housing for use in traffic engineering , ***DE201210107170***, Filing: 03.08.2012, Publication: 15.05.2014

Third-party funding

- International Marie-Curie Fellowship, European Commission, 2014-2017, “Capture of mineral particles by rising bubbles”, 340.000 €
- Graduate Academy of the Technical University of Dresden, 2018-2021, “Investigation of binary particle mixing in intricate three-dimensional apparatuses by advanced ultrafast X-ray computed tomography and high-fidelity simulations”, 48.600 €

Diffuse interface model to simulate the rise of a fluid droplet across a cloud of particles

Gregory Lecrivain,[1,2,*] Yuki Kotani,[1,2] Ryoichi Yamamoto,[2] Uwe Hampel,[1,3] and Takashi Taniguchi[2,†]

[1]*Helmholtz-Zentrum Dresden-Rossendorf, Institut für Fluiddynamik, Bautzner Landstraße 400, 01328 Dresden, Germany*

[2]*Kyoto University, Department of Chemical Engineering, Kyoto 615-8510, Japan*

[3]*Technische Universität Dresden, AREVA-Stiftungsprofessur für Bildgebende Messverfahren für die Energie- und Verfahrenstechnik, 01062 Dresden, Germany*

(Received 1 March 2018; published 25 September 2018)

A large variety of industrial and natural systems involve the adsorption of solid particles to the fluidic interface of droplets in motion. A diffuse interface model is here suggested to directly simulate the three-dimensional dynamics of a fluid droplet rising across a cloud of large particles. In this three-phase model the two solid-fluid boundaries and the fluidic boundary are replaced with smoothly spreading interfaces. The capillary effects and the three-phase flow hydrodynamics are fully resolved. A special treatment is adopted for the interparticle collisions. The effect of the particle concentration on the terminal velocity of a rising fluid droplet is then investigated. It is found that, at low Reynolds number, the terminal velocity of a rising fluid droplet decreases exponentially with the particle concentration. This exponential decay is confirmed by a simple rheological model.

DOI: 10.1103/PhysRevFluids.3.094002

I. INTRODUCTION

A large variety of systems involve the adsorption of solid particles to the fluidic interface of droplets in motion. Important industrial applications include the stabilization of emulsions and foams [1], the armoring of droplets moving in capillary tubes [2], along with the recovery of mineral particles by rising gas bubbles [3,4]. The encapsulation of oceanic air bubbles in a stabilizing organic film of particles is also remarkable phenomenon, for which the addition of a solid constituent drastically changes the dynamics of a natural binary fluid system [5]. The direct numerical simulation of such ternary systems is difficult. This can probably be attributed to the complexity of the mechanism itself, in which capillary effects, three-phase flow hydrodynamics, and interparticle collisions are all intertwined. The majority of the developed three-phase models were used to primarily test the dynamics of a single particle trapped at a planar fluidic interface [6–8]. Some more complex simulations were also performed to study the rearrangement of ellipsoidal particles initially placed at the fluidic interface of an immobile spherical droplet [9,10]. When it comes to simulating the rise of a droplet across a cloud of particles, only a few attempts can be found in the literature. We cite, for instance, the work of van Sint Annaland *et al.* [11], in which the dynamics of a rising gas bubble interacting with a large cloud of pointlike particles were simulated. Sasic *et al.* [12] later suggested particle-resolved simulations in a relatively small ternary system, typically containing no more than five particles. More recently, Bogner *et al.* [13] reported

*g.lecrivain@hzdr.de
†taniguch@cheme.kyoto-u.ac.jp

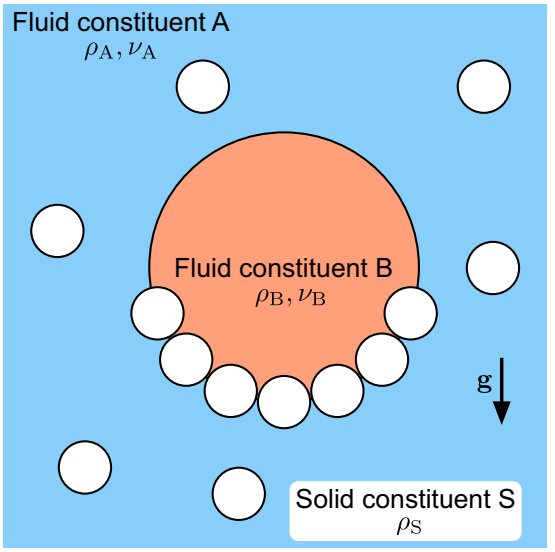

FIG. 1. Schematic of the reference ternary system representing a fluid droplet B rising in the host fluid A. The particles of the solid constituent S adsorb at the fluidic interface of the binary fluid.

particle-resolved simulations of a much larger system, thereby pointing out the growing importance of fully resolved three-phase flow simulations. In a similar way, the aim of this work is the fully resolved and three-dimensional simulation of a rising fluid droplet in a multiparticle system. The diameter of each particle spreads over 10 grid points and that of the bubble over about 50 points. The simulations are performed using a modified diffuse interface model, meaning that the fluidic boundary and the two solid-fluid boundaries are replaced with smoothly spreading interfaces [14]. The three-phase diffuse interface model extends on formulations previously proposed [15–18]. After suggesting an appropriate treatment for the interparticle collisions, found to adversely affected by the diffusivity of the solid-fluid interface, the effect of particle concentration on the terminal velocity of a rising droplet is investigated.

II. SIMULATION MODEL

A. Binary fluid mixture

Suppose a ternary system, in which a dispersed solid constituent representing the particle cloud is immersed in a binary fluid mixture. A schematic of the reference ternary system presently investigated is illustrated in Fig. 1. The capital letter "S" is hereafter introduced to denote a quantity associated with the solid constituent. The field $\phi_S(\mathbf{x}, t)$, where $\mathbf{x}$ is the spatial coordinate and t the time, denotes the volume fraction of the solid constituent. The binary fluid mixture separates into its two immiscible fluid constituents, "A" and "B." The constituent A represents the host fluid and the constituent B the fluid inside the droplet. In a similar fashion, the two volume fractions $\phi_A(\mathbf{x}, t)$ and $\phi_B(\mathbf{x}, t)$ are also introduced. The separation of the binary fluid mixture into its two constituents is driven by the minimization of the free energy

$$\mathcal{F} = \frac{k_B T_0}{v_0} \int_{\mathcal{V}} f(\phi_A, \phi_B, \phi_S)\, d\mathbf{x}, \tag{1}$$

where $\mathcal{V}$ is the region of space occupied by the ternary system, k_B the Boltzmann constant, T_0 the temperature, v_0 a reference unit volume, and f the free energy density scaled by the reference value $e_0 = k_B T_0 / v_0$. The formulation recently suggested by the same authors is here retained for the free

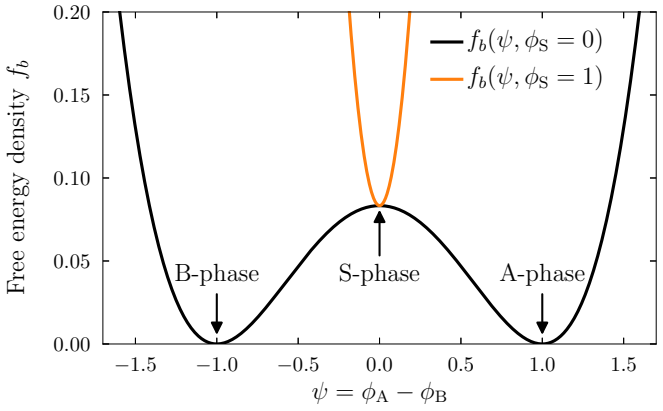

FIG. 2. Bulk component of the free energy density $f_b(\psi, \phi_S)$ inside and outside the solid constituent.

energy density [19,20]. The reader is referred to Appendix A for its exact formulation. Because of the phase summation $\phi_A + \phi_B + \phi_S = 1$, the free energy density is rewritten as $f(\psi, \phi_S)$, where this order parameter is defined as $\psi(\mathbf{x}, t) = \phi_A - \phi_B$. The value of this parameter ψ is obtained from the minimization of the free energy. The bulk component of the free energy density $f_b(\psi, \phi_S)$ is shown in Fig. 2.

Outside of the particle (i.e., $\phi_S = 0$), the free energy has two stable minima. The first minimum is located at $\psi = -1$ (fluid constituent B) and the second minimum at $\psi = 1$ (fluid constituent A). Inside the particle (i.e., $\phi_S = 1$), the free energy changes to a single well function with a minimum located at $\psi = 0$ (solid constituent S). This field ψ is updated in time according to the modified Cahn-Hilliard equation [17]

$$\frac{\partial \psi}{\partial t} + \nabla \cdot [\psi \mathbf{u} - M(\mathbf{I} - \mathbf{n}_S \otimes \mathbf{n}_S) \cdot \nabla \mu] = 0, \tag{2}$$

where M is the mobility, $\mathbf{I}$ the unit tensor, $\mathbf{n}_S = -\nabla\phi_S/|\nabla\phi_S|$ the local unit vector normal to the surface of the solid particle, and $\mu(\psi, \phi_S) = \delta\mathcal{F}/\delta\psi$ the chemical potential. Away from the particle diffuse interface the outer product $\mathbf{n}_S \otimes \mathbf{n}_S$ is set to the zero tensor.

B. Solid constituent

The solid particle cloud forming the solid constituent S is decomposed into a number N_S of spherical particles with identical radius r_s. The lowercase letter $s \in S$ is hereafter used to denote a quantity associated with the sth Lagrangian particle. As one moves from the inner particle region to the outer region, the volume fraction ϕ_s of the sth particle smoothly transitions from unity to zero. A number of smooth profiles are suggested in Ref. [21]. A truncated hyperbolic function, associated with the interfacial distance ξ_S and the cutoff length ξ_c, is presently used to represent the spherical shape of each particle. The exact mathematical expression for $\phi_s(\mathbf{x}, t)$ can be seen in Eq. (B1) of Appendix B. Note that the cutoff length is primarily introduced to speed up the calculation time because it reduces the number of times the hyperbolic function is called. The total volume fraction of the solid constituent is then given by

$$\phi_S(\mathbf{x}, t) = \sum_{s \in S} \phi_s. \tag{3}$$

C. Hydrodynamics

The total velocity field is resolved using the "smooth profile method," which essentially uses a Cartesian grid to solve the Navier-Stokes equations. In this method the total velocity field is decomposed as $\mathbf{u} = (1 - \phi_S)\mathbf{u}_{AB} + \phi_S\mathbf{u}_S$, where the first term is the velocity field of the binary fluid and the second term the solid velocity field. This latter is defined as $\phi_S\mathbf{u}_S = \sum \phi_s[\mathbf{V}_s + \mathbf{\Omega}_s \times (\mathbf{x} - \mathbf{X}_s)]$. Further reading on the smooth profile method can be found in Refs. [21,22]. The total velocity, which satisfies the incompressibility condition $\nabla \cdot \mathbf{u} = 0$, is here given by solving the modified momentum equation

$$\rho\left[\frac{\partial \mathbf{u}}{\partial t} + (\mathbf{u}\cdot\nabla)\mathbf{u}\right] = \nabla\cdot[-p\mathbf{I} + \boldsymbol{\sigma}_v] + \rho\phi_S\mathbf{f}_S + \mathbf{f}_c + \mathbf{f}_g, \tag{4}$$

where $\boldsymbol{\sigma}_v$ is the viscous stress tensor. The first additional term $\mathbf{f}_S$ on the right-hand side of Eq. (4) enforces the particle rigidity. Its exact formulation can be found in the original development of the smooth profile method [21,22]. The second capillary term is given by $\mathbf{f}_c = -\psi\nabla\mu - \phi_S\nabla\mu_S$, where $\mu_S = \delta\mathcal{F}/\delta\phi_S$ [19]. The third gravity term is given by $\mathbf{f}_g = (\rho - \rho_{avg})\mathbf{g}$. The substraction by the space-averaged density $\rho_{avg} = \int\rho(\mathbf{x}, 0)\,d\mathbf{x}/\int d\mathbf{x}$ was previously suggested for buoyancy-driven droplet flows in a periodic domain [23]. The total density and viscosity fields are given by

$$\rho(\mathbf{x}, t) = \phi_A(\mathbf{x}, t)\rho_A + \phi_B(\mathbf{x}, t)\rho_B + \phi_S(\mathbf{x}, t)\rho_S, \tag{5}$$

$$\eta(\mathbf{x}, t) = \phi_A(\mathbf{x}, t)\eta_A + \phi_B(\mathbf{x}, t)\eta_B + \phi_S(\mathbf{x}, t)\eta_S, \tag{6}$$

where the constants $\rho_{i=A,B,S}$ and $\eta_{i=A,B,S}$ are the respective user-defined density and viscosity of each constituent. Note that the two volume fractions ϕ_A and ϕ_B do not actually appear in our implementation, since we introduced the order parameter $\psi(\mathbf{x}, t)$. Hence the viscosity and the density fields are rewritten as $\rho(\psi, \phi_S)$ and as $\nu(\psi, \phi_S)$, respectively. The exact formulations are shown in Appendix C.

D. Multiparticle dynamics

The hydrodynamic force $\mathbf{F}_{hyd}$, the capillary force $\mathbf{F}_{cap}$, the collision force $\mathbf{F}_{col}$, and an external force $\mathbf{F}_{ext}$ acting on each particle are presently retained. The equations for the translational velocity $\mathbf{V}_s = d\mathbf{X}_s/dt$, where $\mathbf{X}_s$ is the position of the sth particle center of mass, and the rotational velocity $\mathbf{\Omega}_s$ are given by [24]

$$m_s\frac{d\mathbf{V}_s}{dt} = \mathbf{F}_{hyd} + \mathbf{F}_{cap} + \mathbf{F}_{col} + \mathbf{F}_{ext}, \tag{7}$$

$$\mathbf{I}_s\frac{d\mathbf{\Omega}_s}{dt} = \mathbf{T}_{hyd} + \mathbf{T}_{cap}, \tag{8}$$

where $m_s = \rho_S\int\phi_s\,d\mathbf{x}$ is the particle mass and $\mathbf{I}_s = \rho_S\mathbf{I}\int\phi_s\boldsymbol{\ell}_s^2\,d\mathbf{x}$ the diagonal inertia tensor, and $\boldsymbol{\ell}_s = \mathbf{x} - \mathbf{X}_s$ the distance vector from the particle center of mass to the spatial coordinate. The term $\mathbf{T}_{hyd}$ is the hydrodynamic torque, and $\mathbf{T}_{cap}$ the capillary torque. The hydrodynamic and the capillary components are directly resolved. Their values are calculated by using a momentum conservation between the solid constituent and the binary fluid mixture. A detailed description of the force and torque calculations can be seen in Appendix D.

1. Depletion layer adjacent to the particle boundary (S1)

The reference system presently studied is composed of a binary fluid mixture, whose fluid constituents A and B are ideally separated by a sharp interface, and by multiple hard-sphere particles S with radii r_s. In this work, however, the three interfaces A/B, A/S, and B/S are no longer sharp but are replaced with smoothly spreading interfaces of user-defined thicknesses, which correspond to

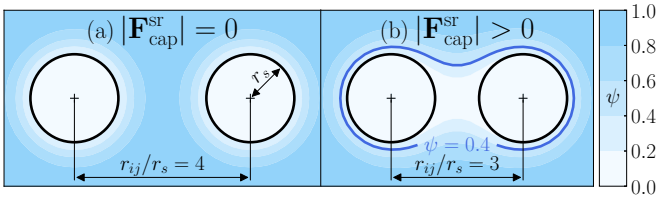

FIG. 3. Depletion layers adjacent to the boundaries of two solid particles immersed in the host consistent A (a). The two particles are pinned. Upon a close encounter, the depletion layers deform, and the two particles attract each other because of a short-range capillary force $\mathbf{F}^{\rm sr}_{\rm cap}$ (b).

given interfacial energies. Most of the particles are suspended in the host fluid. As one moves from the host fluid constituent A to the particle inner region S, the order parameter ψ smoothly transitions from unity to zero. This leads to the formation of a depletion layer across the solid particle boundary [Fig. 3(a)].

In a multiple particle system, as is the case here, this depletion layer induces an undesired capillary attraction. As two particles come close to each other, their respective depletion layers tend to locally deform [Fig. 3(b)]. Subsequently, a short-range capillary force $\mathbf{F}^{\rm sr}_{\rm cap}$ arises. This scenario, reminiscent of the liquid bridge bonding particles together [25,26], is an inevitable disadvantage occurring when working with a diffuse interface model. The distance, at which the short-range capillary force activates, here has a value comparable to that of the particle size, and so an affordable computational cost is achieved. The undesired effect caused by the short-range attraction force $\mathbf{F}^{\rm sr}_{\rm cap}$ can be further reduced by setting a smaller ratio of the interfacial thickness to the particle radius. Counteracting this short-range capillary attraction is a central aspect of this work. We suggest implementing the repulsive collision force acting on the ith particles as $\mathbf{F}_{\rm col} = -(\mathbf{F}^{\rm sr}_{\rm cap} + \nabla U_{ij})$, where $\mathbf{F}^{\rm sr}_{\rm cap}$ is calculated using a preliminary set of simulations (detailed in the result section) and U_{ij} is a truncated Lennard-Jones potential [27]. The potential takes the form

$$U_{ij} = \begin{cases} 4\epsilon\left[\left(\frac{\sigma}{r_{ij}}\right)^{12} - \left(\frac{\sigma}{r_{ij}}\right)^{6}\right] & \text{if } r_{ij} < r_c \\ 0 & \text{elsewhere} \end{cases}, \tag{9}$$

where ϵ is the depth of the potential well, $r_{ij} = |\mathbf{X}_i - \mathbf{X}_j|$ the separation distance between the center of masses of the ith and the jth particles, $\sigma = 2r_s + \xi_c$ the distance at which the interparticle potential equates zero, and $r_c = 2^{1/6}\sigma$ the cutoff distance. The truncation suppresses the attractive part of the potential.

III. RESULTS

The governing equations were implemented in their nondimensional form using the Reynolds number Re, the Péclet number Pe, and the capillary number Ca. These three nondimensional numbers are defined as

$$\mathrm{Re} = \frac{\rho_0 U_0 L_0}{\eta_0}, \quad \mathrm{Pe} = \frac{U_0 L_0}{D_0}, \quad \mathrm{Ca} = \frac{\eta_0 U_0}{\gamma_0}, \tag{10}$$

where $\rho_0 = \rho_{\rm A}$ and $\eta_0 = \eta_{\rm A}$ are the density and the viscosity of the host fluid constituent A, respectively. The reference velocity is set to $U_0 = \sqrt{gL_0}$. The reference length is defined as $L_0 = \xi$, the diffusion coefficient as $D_0 = e_0 M$, and the reference surface tension as $\gamma_0 = e_0 L_0$. This nondimensionalization is similar to that used in previous studies on phase separation [28,29]. For the sake of conciseness, the procedure implemented to solve the governing equations is found in Appendix D. Using the present implementation, a fluid density ratio up to $\rho_{\rm A}/\rho_{\rm B} = 40$ can be achieved. The resulting droplet Reynolds and Eötvös numbers are calculated, based on the droplet radius r_b, as $\mathrm{Re}_b = \rho_{\rm A} r_b \sqrt{g r_b}/\eta_{\rm A} = 0.98$ and $\mathrm{Eo}_b = \rho_{\rm A} g r_b^2/\gamma_0 = 0.23$ for all subsequent

TABLE I. Input parameters used in the simulation sets. The term Δ is the size of a grid element and N the number of grid nodes. In S3, S4, and S5, the Eötvös droplet numbers, Eo_b, and the Reynolds droplet number, Re_b, are set to constant values.

	Binary fluid mixture						Solid constituent						Collision		Dimensionless numbers			Grid	
	$\frac{\xi_A}{\xi}$	$\frac{\xi_B}{\xi}$	χ	$\frac{\rho_A}{\rho_B}$	$\frac{\eta_A}{\eta_B}$	$\frac{r_b}{\xi}$	$\frac{\xi_s}{\xi}$	$\frac{\xi_c}{\xi}$	$\frac{\rho_S}{\rho_A}$	$\frac{\eta_S}{\eta_A}$	$\frac{r_s}{\xi}$	N_S	$\frac{\sigma}{\xi}$	$\frac{\epsilon}{\gamma_0 \xi^2}$	Pe	$\frac{\mathrm{Re}}{100}$	$\frac{\mathrm{Ca}}{100}$	$\frac{\Delta}{\xi}$	N
S1	1	1	8/3	[1-40]	1	18.3	–	–	–	–	–	0	–	–	1	1	5	1	128^3
S2	1	1	8/3	–	–	–	3	3.6	1	1	5	2	13.6	0.5	1	1	5	1	128^3
S3	1	1	8/3	10	1	[16,42.6]	3	3.6	1	1	[3.75,10]	22	[11.1,23.6]	0.5	1	[1.54,0.35]	[5.77,3.53]	1	$[90^2, 256^2]$
S4	1	1	8/3	10	1	26.6	3	3.6	1	1	6.25	[0-300]	16.1	0.5	1	0.72	4.47	1	$160^2, 160^3$
S5	1	1	8/3	10	1	[16-42.6]	3	3.6	1	1	[3.75-10]	22	[11.1,23.6]	0.5	1	[1.54-0.35]	[5.77-3.53]	1	$[90^2$-$256^2]$

simulations. These two numbers, commonly used to characterize the shape of rising gas bubbles in water [30], indicate that the rising droplet remains spherical throughout its ascension, thereby avoiding the ellipsoidal bubble regime. All the subsequent results are presented for two-dimensional and three-dimensional test cases.

A. Rising droplet in the absence of particles (S1)

First the terminal velocity of a rising droplet in a periodic domain is validated (simulation set S1). There are no particles in the system. The input parameters used in simulation set S1 are shown in Table I. In the Stokes regime, i.e., at low droplet Reynolds and Eötvös numbers, the spherical droplet only slightly deforms during its rise. This allows us to compare the simulated droplet terminal velocity $\mathbf{U}_b^{\mathrm{sim}} = \int \phi_B \mathbf{u}\, d\mathbf{x} / \int \phi_B\, d\mathbf{x}$ with its theoretical counterpart $\mathbf{U}_b^{\mathrm{th}}$ [31,32]. The derivation of the theoretical terminal droplet velocity is described in Appendix E. Previous experimental and numerical data have shown that, up to a Reynolds number $\mathrm{Re}_b < 2$, the drag coefficient of a spherical rising droplet is within the well-known drag curves for solid spheres and inviscid spherical bubbles, respectively $\mathrm{C}_d = 24/\mathrm{Re}_b$ and $\mathrm{C}_d = 16/\mathrm{Re}_b$ [33]. In the present investigated regime, the rising droplet remains fairly spherical. The Eötvös droplet number, $\mathrm{Eo}_b < 1$, and the Reynolds droplet number, $\mathrm{Re}_b < 2$, are set to low values. It is therefore fair to compare the data with a laminar stokes drag, which we corrected due to the periodicity imposed on each side of the domain. Figure 4 shows the error in the droplet terminal velocity as a function of the fluid density ratio.

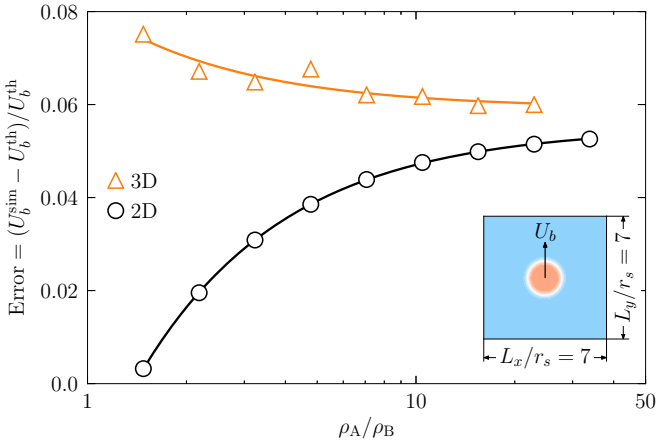

FIG. 4. Error in the terminal velocity of a rising spherical bubble in the absence of particles. Periodicity is enforced on all side boundaries of the domain.

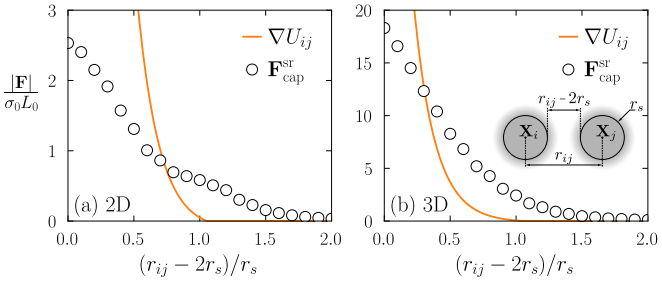

FIG. 5. Short-range capillary force $\mathbf{F}^{\rm sr}_{\rm cap}$ calculated as a function of the normalized particle separation distance r_{ij}. The two particles are pinned and immersed in the fluid constituent A. The repulsive force $-\boldsymbol{\nabla} U_{ij}$ is also shown.

It is seen that a good agreement is achieved for $\rho_{\rm A}/\rho_{\rm B} > 10$. An error of about 6% is achieved in a two-dimensional and a three-dimensional domain. Note that the error is also dependent on the interfacial thicknesses ξ, $\xi_{\rm A}$, and $\xi_{\rm B}$ [21]. Although it not shown here, the deformation of the droplet was also found to compare qualitatively well with the data of Hysing *et al.* [34] at higher capillary numbers.

B. Rising droplet in the presence of particles

1. Calculation of the short-range capillary force (S2)

At this stage the short-range capillary force $\mathbf{F}^{\rm sr}_{\rm cap}$ is still unknown. Hence a second of set of simulations S2, in which two pinned particles are immersed in the host fluid constituent A, is performed. As seen in Table I, the depth of the potential wall ϵ is arbitrarily set to a constant value throughout the subsequent simulations. Figure 5 shows the evolution of the short-range capillary force calculated as a function of the particle separation distance $r_{ij} - 2r_s$.

It is seen that the short-range capillary force decays exponentially with the separation distance. This finding is in line with previously reported data [17]. The magnitude of the repulsive force $-\boldsymbol{\nabla} U_{ij}$, derived from the Lennard-Jones potential in Eq. (9), is also shown.

2. Suppression of the clustering effect (S3)

The effect of the corrected collision force $\mathbf{F}_{\rm col} = -(\mathbf{F}^{\rm sr}_{\rm cap} + \boldsymbol{\nabla} U_{ij})$ on a multiparticle system is here briefly tested in simulation set S3. At the initial time $t = 0$, the particles are randomly placed in the host fluid constituent A, and the droplet is placed at the center of the domain. The particles have the same density as that of the host fluid, i.e., $\rho_{\rm S}/\rho_{\rm A} = 1$. Figure 6 shows the effect of the corrected collision force on a multiparticle system.

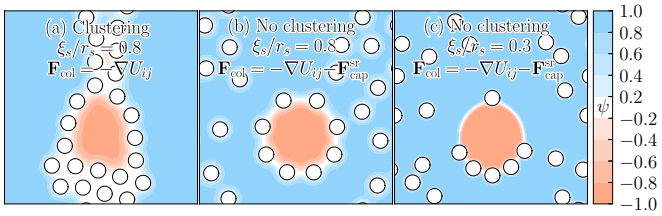

FIG. 6. Effect of the corrected collision force in a multiparticle system. In panel (a) clustering occurs as opposed to panel (b). The solid lines correspond to the reference particle radius r_s. In panel (c) the ratio of the interfacial thickness to the particle radius is decreased. The simulations are performed with $N_{\rm S} = 23$ particles.

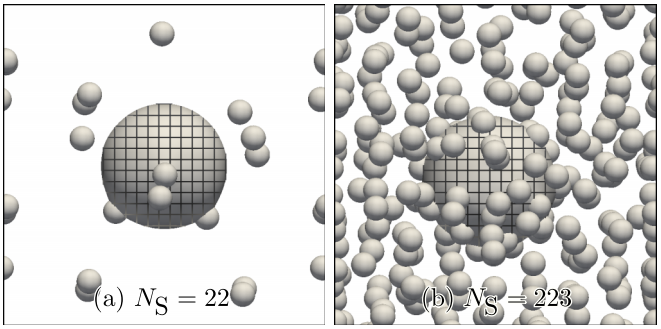

FIG. 7. Snapshot of the three-dimensional rising bubble in a multiparticle system: (a) low particle concentration; (b) high particle concentration.

In case (a), the collision force is too weak to overcome the short range capillary force, hence particle clustering occurs. In case (b), the clustering is suppressed. As expected the particles are eventually collected at the fluidic interface of the rising droplet. After the rising droplet is completely armored, the surrounding particles suspended in the host fluid constituent A were found to move around and avoid the rising particle-droplet aggregate. In case (c), the ratio of the interfactial thickness to the particle radius is decreased. A convergence study (Appendix F) showed that for a ratio below $\xi_s/r_s < 0.4$ the results become grid independent.

3. Effect of particle concentration (S4)

In simulation set S4, the number of particles suspended in the domain is varied. Figure 7 shows the three-dimensional rising droplet at low total solid fraction [Fig. 7(a)] and at high solid fraction [Fig. 7(b)]. See the Supplemental Material [35] for a typical animation of a droplet rising across a particle cloud.

The fluidic interface of the droplet is defined as the isosurface $\psi = 0$. The mean bubble velocity and its deviation are then calculated as a function of the number of particles. The statistics are averaged over two flow-through times, with one flow-through time being the time it takes for the droplet to traverse the domain height. Figure 8 shows the terminal velocity of the rising droplet as a function of the solid concentration in the host fluid.

The concentration of the solid constituent suspended in the host fluid, which essentially is a conversion of the number of particles suspended in A, is calculated as $\langle \phi_S \rangle = \int \phi_S \, d\mathbf{x} / \int \phi_A \, d\mathbf{x}$. It is found that the terminal velocity U_b of the droplet decreases exponentially with increasing solid concentration. This decrease is backed up quantitatively by the recent numerical and experimental

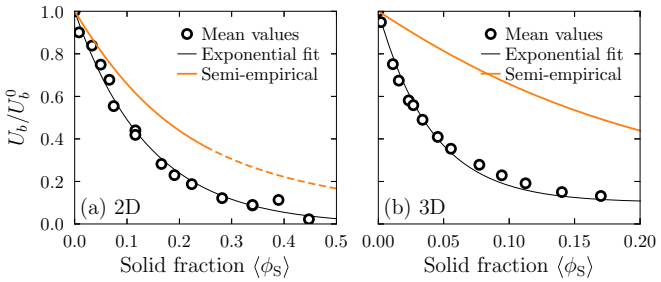

FIG. 8. Effect of the solid concentration in the host fluid on the terminal velocity of a rising bubble in the Stokes regime. The standard deviation of the mean bubble velocity is about as large as the symbols. The semiempirical expression, obtained with $\lambda_0 = 4$ and $\lambda_1 = 12$, is extrapolated beyond its range of validity.

observations [36,37]. For illustration purposes, an exponential fit was added to the figure. The exponential fit takes the form $U_b/U_b^0 = 1 - \alpha(1 - e^{-\langle\phi_S\rangle/\beta})$, where α and β are two best-fit values, and U_b^0 equates the terminal velocity of the droplet in the absence of particles. With the present best-fit function, the droplet velocity ratio equals unity for $\langle\phi_S\rangle = 0$. With higher solid fraction, i.e., for $\langle\phi_S\rangle \to 1$, the droplet terminal velocity converges to the constant value $U_b/U_b^0 = 1 - \alpha$. In the present simulations, α equates to a value close to unity. It may, however, take a greater value, should the bubble move downwards because of the gravity. A direct comparison with data taken from the literature is difficult because the few available studies considered the rising of highly deformable air bubbles in water [37]. The simulations are here performed with a smaller density ratio. Based on a the rheological model of Hooshyar *et al.* [36], we derive semiempirical values for the terminal droplet velocity rising across a suspension of particles. In the semidilute regime, i.e., for $\langle\phi_S\rangle < 0.25$, the apparent viscosity of the suspension A/S takes the polynomial form

$$\frac{\eta_{AS}}{\eta_A} = 1 + \lambda_0\langle\phi_S\rangle + \lambda_1\langle\phi_S\rangle^2, \tag{11}$$

where $1.5 < \lambda_0 < 5$ and $7.35 < \lambda_1 < 14.1$ [38]. In the dilute regime, restricted to $\langle\phi_S\rangle < 0.02$, the above equation simplifies to the well-established analytical expression $\eta_{AS}/\eta_A = 1 + 2.5\langle\phi_S\rangle$ [39]. By substituting the viscosity of the host fluid in Eq. (E1) with the apparent viscosity η_{AS}, a semiempirical terminal velocity can be estimated. While this semiempirical value does not take into account the particle attachment to the fluidic interface of the rising droplet, it does confirm the exponential decay presently observed.

IV. CONCLUSIONS

A diffuse interface model is suggested to directly simulate the dynamics of a rising droplet in the presence of large particles. An advantage of the method lies in the fact that the capillary effects and the three-phase flow hydrodynamics are resolved. An appropriate repulsive interparticle collision force has been suggested to counteract the short-range capillary attraction caused by the depletion layer adjacent to the particle boundary. This short-range capillary attraction, even though its effect can be diminished with a finer grid resolution, is inevitable when employing a diffuse interface model. In a second stage the effect of the particle concentration on the terminal velocity of a rising fluid droplet is investigated. We have found that, in the Stokes regime, the bubble terminal velocity decreases exponentially with the particle concentration. Further work will include an appropriate extension of the current model to achieve large density and viscosity ratios similar to those observed in industrial air-water systems.

ACKNOWLEDGMENTS

This work was supported by a Marie Curie International Outgoing Fellowship with the European Union Seventh Framework Program for Research and Technological Development (2007–2013) under the grant agreement number 623518.

APPENDIX A: FREE ENERGY DENSITY

The free energy density is here given by

$$f = f_b + \frac{\xi^2}{2}|\nabla(\phi_A - \phi_B)|^2 + \frac{\xi_A^2}{2}|\nabla(\phi_A - \phi_S)|^2 + \frac{\xi_B^2}{2}|\nabla(\phi_B - \phi_S)|^2, \tag{A1}$$

where $f_b = -A(\phi_S)\psi^2/2 + B(\phi_S)\psi^4/4$ [19,20]. The two polynomial expressions $A(\phi_S)$ and $B(\phi_S)$ are derived from a fourth-order expansion of the logarithmic expression $f_b = \phi_A \ln(\phi_A) + \phi_B \ln(\phi_B) + \chi\phi_A\phi_B$, where χ is a parameter describing the affinity between the two fluid constituents. The three tunable interfacial length scales ξ, ξ_A, and ξ_B preceding the gradient terms are introduced to control the particle wettability.

APPENDIX B: SMOOTH PARTICLE PROFILE

The following mathematical function is used to represent the spherical shape of the sth particle:

$$\phi_s(\mathbf{x}) = \begin{cases} 1 & \text{if} |\boldsymbol{\ell}_s| < r_s - \frac{\xi_c}{2} \\ 0 & \text{if} |\boldsymbol{\ell}_s| > r_s + \frac{\xi_c}{2}, \\ \frac{1}{2}\tanh\left(\frac{r_s - |\boldsymbol{\ell}_s|}{\xi_s/2}\right) + \frac{1}{2} & \text{elsewhere} \end{cases} \tag{B1}$$

where r_s is the particle radius, $\boldsymbol{\ell}_s(\mathbf{x}) = \mathbf{x} - \mathbf{X}_s$ the distance vector from the center of mass $\mathbf{X}_s$ of the sth particle to the spatial coordinate $\mathbf{x}$, and ξ_c the cutoff length.

APPENDIX C: DENSITY AND VISCOSITY FIELDS

The volume fractions ϕ_A and ϕ_B do not actually appear in our implementation, since we introduced the order parameter $\psi(\mathbf{x}, t)$. Since we define $\psi = \phi_\mathrm{A} - \phi_\mathrm{B}$ and $\phi_\mathrm{A} + \phi_\mathrm{B} + \phi_\mathrm{S} = 1$, the two volume fractions are given by $\phi_\mathrm{A} = (1 + \psi - \phi_\mathrm{S})/2$ and $\phi_\mathrm{B} = (1 - \psi - \phi_\mathrm{S})/2$. In this way, the total density field is recast as

$$\rho(\psi, \phi_\mathrm{S}) = \left(\frac{\rho_\mathrm{A} + \rho_\mathrm{B}}{2}\right) + \left(\frac{\rho_\mathrm{A} - \rho_\mathrm{B}}{2}\right)\psi + \left(\rho_\mathrm{S} - \frac{\rho_\mathrm{A} + \rho_\mathrm{B}}{2}\right)\phi_\mathrm{S}. \tag{C1}$$

In the absence of a particle, i.e., $\phi_\mathrm{S} = 0$, the density reduces to $\rho(\psi = 1, 0) = \rho_\mathrm{A}$ in the fluid A and to $\rho(\psi = -1, 0) = \rho_\mathrm{B}$ in fluid B. While inside the particle, i.e., $\phi_\mathrm{S} = 1$, the density reduces to $\rho(\psi = 0, 1) = \rho_\mathrm{S}$. Across an interface, the density smoothly transitions. Similar conclusions can be drawn for the density.

APPENDIX D: NUMERICAL METHOD

The numerical method is briefly described. For a more complete description the reader is referred to our previous work [19–21]. Let ψ^n be the order parameter at the time t^n. The field ψ^{n+1} is first advanced in time using a forward Euler method as

$$\psi^{n+1} = \psi^n - \int_{t^n}^{t^{n+1}} \nabla \cdot \mathbf{J}^n dt, \tag{D1}$$

where $\mathbf{J}^n = \psi^n \mathbf{u}^n - M(\mathbf{I} - \mathbf{n}_\mathrm{S}^n \otimes \mathbf{n}_\mathrm{S}^n) \cdot \nabla \mu^n$. The position of each center of mass $\mathbf{X}_s$ along with the quaternion $\mathbf{Q}_s$ associated with the sth solid particle is then updated in time as

$$\mathbf{X}_s^{n+1} = \mathbf{X}_s^n + \int_{t^n}^{t^{n+1}} \mathbf{V}_s^n \, dt, \tag{D2}$$

$$\mathbf{Q}_s^{n+1} = \mathbf{Q}_s^n + \frac{1}{2}\int_{t^n}^{t^{n+1}} \mathbf{A}_s^n \cdot \mathbf{Q}_s^n \, dt, \tag{D3}$$

where $\mathbf{A}_s(\boldsymbol{\Omega}_s)$ is a 4×4 orthogonal matrix function of the particle rotational velocity [20]. After updating all the solid volume fractions $\phi_{s\in\mathrm{S}}^{n+1}$ [Eq. (B1)] and the summation ϕ_S^{n+1} [Eq. (3)], the density field η^{n+1} and the viscosity field ρ^{n+1} can be advanced in time using Eq. (C1). A fractional step approach is employed here to solve the momentum equation (4). An intermediate velocity is first calculated as

$$\mathbf{u}^* = \mathbf{u}^n + \int_{t^n}^{t^{n+1}} \left\{ -(\mathbf{u}^n \cdot \nabla)\mathbf{u}^n + \frac{1}{\rho^{n+1}}\left[\nabla \cdot \left(-p^*\mathbf{I} + \boldsymbol{\sigma}_\mathrm{v}^n\right) - \psi^{n+1}\nabla\mu^{n+1}\right] \right\} dt, \tag{D4}$$

where p^* is an intermediate pressure calculated by solving a Poisson equation $\nabla \cdot \mathbf{u}^* = 0$ and $\boldsymbol{\sigma}_\mathrm{v}^n = \eta^{n+1}[\nabla\mathbf{u}^n + (\nabla\mathbf{u}^n)^\top]$ is the viscous stress tensor. A successive over-relaxation method is employed here to solve the Poisson equation. Note that this solver along with some of the discretization

schemes used in the modified Cahn-Hilliard equation are not optimal. The implementation of a more advanced numerical procedure [40] is, however, well involved. The translational and rotational velocities of the each particle are then updated in time as

$$\mathbf{V}_s^{n+1} = \mathbf{V}_s^n + \frac{1}{m_s}\int_{t^n}^{t^{n+1}} \Big(\sum \mathbf{F}\Big) dt, \tag{D5}$$

$$\mathbf{\Omega}_s^{n+1} = \mathbf{\Omega}_s^n + \mathbf{I}_s^{-1} \cdot \int_{t^n}^{t^{n+1}} \Big(\sum \mathbf{T}\Big) dt. \tag{D6}$$

The hydrodynamic force and torque are derived by assuming a momentum conservation between the particle and the binary fluid. Since the hydrodynamic and the capillary contributions are accounted for in the calculation of the intermediate velocity, the following two time integrals are given by

$$\int_{t^n}^{t^{n+1}} (\mathbf{F}_{\text{hyd}} + \mathbf{F}_{\text{cap}}) dt = \int_{\mathcal{V}} \rho^{n+1} (\delta \mathbf{u}_s^*)\, d\mathbf{x}, \tag{D7}$$

$$\int_{t^n}^{t^{n+1}} (\mathbf{T}_{\text{hyd}} + \mathbf{T}_{\text{cap}}) dt = \int_{\mathcal{V}} \rho^{n+1} \boldsymbol{\ell}_s^{n+1} \times (\delta \mathbf{u}_s^*)\, d\mathbf{x}, \tag{D8}$$

where $\delta \mathbf{u}_s^* = \phi_s^{n+1}(\mathbf{u}^* - \mathbf{u}_s^*)$ and $\mathbf{u}_s^* = \mathbf{V}_s^n + \mathbf{\Omega}_s^n \times \boldsymbol{\ell}_s^{n+1}$. Finally the velocity field of the entire Lagrangian particle cloud is enforced onto the total fluid velocity field as

$$\mathbf{u}^{n+1} = \mathbf{u}^* + \int_{t^n}^{t^{n+1}} \left(-\frac{1}{\rho^{n+1}} \nabla p_{\text{S}} + \phi_{\text{S}} \mathbf{f}_{\text{S}}\right) dt, \tag{D9}$$

where the pressure p_{S} is obtained from the incompressibility condition $\nabla \cdot \mathbf{u}^{n+1} = 0$. The time integral of the force density field is calculated as

$$\int_{t^n}^{t^{n+1}} \phi_{\text{S}} \mathbf{f}_{\text{S}}\, dt = \phi_{\text{S}}^{n+1} \big(\mathbf{u}_{\text{S}}^{n+1} - \mathbf{u}^*\big), \tag{D10}$$

where $\phi_{\text{S}}^{n+1}\mathbf{u}_{\text{S}}^{n+1} = \sum \phi_s^n (\mathbf{V}_s^{n+1} + \mathbf{\Omega}_s^{n+1} \times \boldsymbol{\ell}_s^{n+1})$.

APPENDIX E: THEORETICAL TERMINAL BUBBLE VELOCITY

The theoretical terminal velocity U_b^{th} of a spherical bubble with radius r_b rising in a cubic periodic domain is calculated as

$$\frac{U_b^{\text{th}}|_{3\text{D}}}{|\mathbf{F}_{\text{ext}}|/(6\pi \eta_{\text{A}} r_b)} = 1 - 1.7601 c^{1/3} + c - 1.5593 c^2, \tag{E1}$$

where $c = \int \phi_{\text{B}}\, d\mathbf{x} / \int d\mathbf{x}$ is the fraction of space occupied by the bubble volume and $\mathbf{F}_{\text{ext}} = (\rho_{\text{B}} - \rho_{\text{A}})\mathbf{g} \int \phi_{\text{B}}\, d\mathbf{x}$ is the external buoyancy force [31]. In a two-dimensional periodic square domain, the theoretical terminal velocity is given by

$$\frac{U_b^{\text{th}}|_{2\text{D}}}{|\mathbf{F}_{\text{ext}}|/(4\pi \eta_{\text{A}} L_0)} = -0.5 \log(c) - 0.738 + c. \tag{E2}$$

The above expressions are valid for $c < 0.25$ [32].

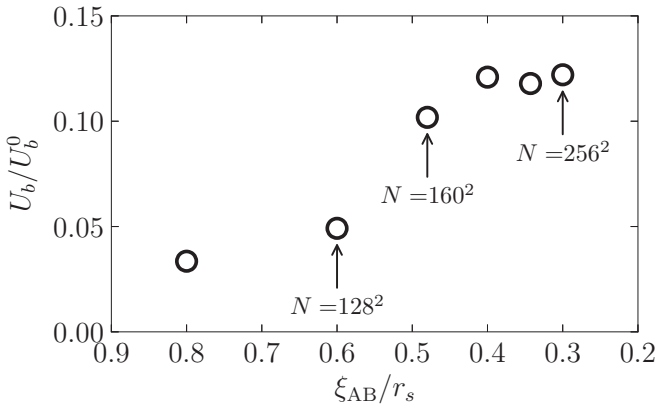

FIG. 9. Effect of the interfacial-length-to-particle-radius ξ_{AB}/r_s on the terminal velocity of a rising droplet. The two-dimensional convergence study was performed with $N_S = 22$ particles.

APPENDIX F: CONVERGENCE STUDY (S5)

We first recall that the field ψ, associated with the A/B interface, varies over the interfacial length [20],

$$\xi_{AB} = \sqrt{\frac{4\xi^2 + \xi_A^2 + \xi_B^2}{\chi - 2}}, \tag{F1}$$

and each solid fraction ϕ_s over the distance ξ_s. These two interfacial lengths here have equal values, i.e., they are set to $\xi_{AB} = \xi_s = 3\Delta$, where Δ is the grid spacing. In the following convergence study, the ratio of the interfacial length to the particle radius ξ_{AB}/r_s is gradually decreased to approach the sharp interface limit. For each simulation in set S5, we set the droplet Reynolds number to $\mathrm{Re}_b = 0.98$ and the Etövös number to $\mathrm{Eo}_b = 0.23$. As seen in Fig. 9, below a ratio $\xi_{AB}/r_s < 4$, the terminal velocity is no longer affected by the grid density. In the simulations presented in the paper, we chose a grid resolution of $N = 160^2$ in two dimensions and $N = 160^3$ in three dimensions, since it reached a good trade-off between computational cost and result accuracy.

[1] N. Taccoen, F. Lequeux, D. Z. Gunes, and C. N. Baroud, Probing the Mechanical Strength of an Armored Bubble and its Implication to Particle-Stabilized Foams, Phys. Rev, X **6**, 011010 (2016).

[2] Y. E. Yu, S. Khodaparast, and H. A. Stone, Armoring confined bubbles in the flow of colloidal suspensions, Soft Matter **13**, 2857 (2017).

[3] S. Y. Tan, S. Ata, and E. J. Wanless, Direct observation of individual particle armored bubble interaction, stability, and coalescence dynamics, J. Phys. Chem. B **117**, 8579 (2013).

[4] G. Lecrivain, G. Petrucci, M. Rudolph, U. Hampel, and R. Yamamoto, Attachment of solid elongated particles on the surface of a stationary gas bubble, Int. J. Multiphase Flow **71**, 83 (2015).

[5] B. D. Johnson and R. C. Cooke, Generation of stabilized microbubbles in seawater, Science **213**, 209 (1981).

[6] K. Stratford, R. Adhikari, I. Pagonabarraga, and J. C. Desplat, Lattice Boltzmann for binary fluids with suspended colloids, J. Stat. Phys. **121**, 163 (2005).

[7] G. B. Davies, T. Kruger, P. V. Coveney, and J. Harting, Detachment energies of spheroidal particles from fluid-fluid interfaces, J. Chem. Phys. **141**, 154902 (2014).

[8] H. I. Mehrabian, J. Harting, and J. H. Snoeijer, Soft particles at a fluid interface, Soft Matter **12**, 1062 (2016).
[9] T. Krüger, S. Frijters, F. Günther, B. Kaoui, and J. Harting, Numerical simulations of complex fluid-fluid interface dynamics, Eur. Phys. J.: Spec. Top. **222**, 177 (2013).
[10] X. C. Luu and A. Striolo, Ellipsoidal Janus nanoparticles assembled at spherical oil/water interfaces, J. Phys. Chem. B **118**, 13737 (2014).
[11] M. van Sint Annaland, N. G. Deen, and J. A. M. Kuipers, Numerical simulation of gas-liquid-solid flows using a combined front tracking and discrete particle method, Chem. Eng. Sci. **60**, 6188 (2005).
[12] S. Sasic, E. K. Sibaki, and H. Ström, Direct numerical simulation of a hydrodynamic interaction between settling particles and rising microbubbles, Eur. J. Mech. B **43**, 65 (2014).
[13] S. Bogner, J. Harting, and U. Rüde, Direct simulation of liquid-gas-solid flow with a free surface lattice Boltzmann method, Intl. J. Comput. Fluid Dyn. **31**, 463 (2017).
[14] D. M. Anderson, G. B. McFadden, and A. A. Wheeler, Diffuse interface model methods in fluid mechanics, Annu. Rev. Fluid Mech. **30**, 139 (1998).
[15] T. Araki and H. Tanaka, Wetting-induced depletion interaction between particles in a phase-separating liquid mixture, Phys. Rev. E **73**, 061506 (2006).
[16] P. C. Millett and Y. U. Wang, Diffuse-interface field approach to modeling arbitrarily-shaped particles at fluid-fluid interfaces, J. Colloid Interface Sci. **353**, 46 (2011).
[17] H. Shinto, Computer simulation of wetting, capillary forces, and particle-stabilized emulsions: From molecular-scale to mesoscale modeling, Adv. Powder Tech. **23**, 538 (2012).
[18] T. Cheng and Y. U. Wang, Shape-anisotropic particles at curved fluid interfaces and role of Laplace pressure: A computational study, J. Colloid Interface Sci. **402**, 267 (2013).
[19] G. Lecrivain, R. Yamamoto, U. Hampel, and T. Taniguchi, Direct numerical simulation of a particle attachment to an immersed bubble, Phys. Fluids **28**, 083301 (2016).
[20] G. Lecrivain, R. Yamamoto, U. Hampel, and T. Taniguchi, Direct numerical simulation of an arbitrarily shaped particle at a fluidic interface, Phys. Rev. E **95**, 063107 (2017).
[21] Y. Nakayama and R. Yamamoto, Simulation method to resolve hydrodynamic interactions in colloidal dispersions, Phys. Rev. E **71**, 036707 (2005).
[22] J. Molina and R. Yamamoto, Direct numerical simulations of rigid body dispersions. I. Mobility/friction tensors of assemblies of spheres, J. Chem. Phys. **139**, 234105 (2013).
[23] A. Esmaeeli and G. Tryggvason, A direct numerical simulation study of the buoyant rise of bubbles at O(100) Reynolds number, Phys. Fluids **17**, 093303 (2005).
[24] G. Lecrivain, R. Rayan, A. Hurtado, and U. Hampel, Using quasi-DNS to investigate the deposition of elongated aerosol particles in a wavy channel flow, Comput. Fluids **124**, 78 (2016).
[25] G. Bournival, S. Ata, and E. J. Wanless, The roles of particles in multiphase processes: Particles on bubble surfaces, Adv. Colloid Interf. Sci. **225**, 114 (2015).
[26] X. Sun and M. Sakai, Direct numerical simulation of gas-solid-liquid flows with capillary effects: An application to liquid bridge forces between spherical particles, Phys. Rev. E **94**, 063301 (2016).
[27] D. S. Bolintineanu, G. S. Grest, J. B. Lechman, F. Pierce, S. J. Plimpton, and P. R. Schunk, Particle dynamics modeling methods for colloid suspensions, Comput. Particle Mech. **1**, 321 (2014).
[28] R. Chella and J. Vinals, Mixing of a two-phase fluid by cavity flow, Phys. Rev. E **53**, 3832 (1996).
[29] V. E. Badalassi, H. D. Ceniceros, and S. Banerjee, Computation of multiphase systems with phase field models, J. Comput. Phys. **190**, 371 (2003).
[30] M. K. Tripathi, K. C. Sahu, and R. Govindarajan, Dynamics of an initially spherical bubble rising in quiescent liquid, Nat. Commun. **6**, 6268 (2015).
[31] H. Hasimoto, On the periodic fundamental solutions of the Stokes equations and their application to viscous flow past a cubic array of spheres, J. Fluid Mech. **5**, 317 (1959).
[32] A. S. Sangani and A. Acrivos, Slow flow through a periodic array of spheres, Int. J. Multiphase Flow **8**, 343 (1982).
[33] F. Raymond and J. M. Rosant, A numerical and experimental study of the terminal velocity and shape of bubbles in viscous liquids, Chem. Eng. Sci. **55**, 943 (2000).

[34] S. Hysing, S. Turek, D. Kuzmin, N. Parolini, E. Burman, S. Ganesan, and L. Tobiska, Quantitative benchmark computations of two-dimensional bubble dynamics, Intl. J. Numer. Methods Fluids **60**, 1259 (2009).

[35] See Supplemental Material at http://link.aps.org/supplemental/10.1103/PhysRevFluids.3.094002 for three-dimensional simulation of a droplet rising across a particle cloud.

[36] N. Hooshyar, J. R. van Ommen, P. J. Hamersma, S. Sundaresan, and R. F. Mudde, Dynamics of Single Rising Bubbles in Neutrally Buoyant Liquid-Solid Suspensions, Phys. Rev. Lett. **110**, 244501 (2013).

[37] M. W. Baltussen, J. A. M. Kuipers, and N. G. Deen, Direct numerical simulation of effective drag in dense gas-liquid-solid three-phase flows, Chem. Eng. Sci. **158**, 561 (2017).

[38] S. Mueller, E. W. Llewellin, and H. M. Mader, The rheology of suspensions of solid particles, Proc. R. Soc. London A **466**, 1201 (2010).

[39] A. Einstein, Berichtigung zu meiner Arbeit: Eine neue Bestimmung der Moleküldimensionen, Ann. Phys. **339**, 591 (1911).

[40] M. Fujita, O. Koike, and Y. Yamaguchi, Direct simulation of drying colloidal suspension on substrate using immersed free surface model, J. Comput. Phys. **281**, 421 (2015).